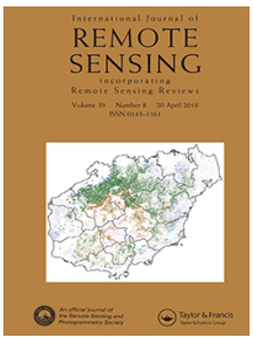

International Journal of Remote Sensing

ISSN: 0143-1161 (Print) 1366-5901 (Online) Journal homepage: http://www.tandfonline.com/loi/tres20

SAR-based detection of flooded vegetation – a review of characteristics and approaches

Viktoriya Tsyganskaya, Sandro Martinis, Philip Marzahn & Ralf Ludwig

To cite this article: Viktoriya Tsyganskaya, Sandro Martinis, Philip Marzahn & Ralf Ludwig (2018) SAR-based detection of flooded vegetation – a review of characteristics and approaches, International Journal of Remote Sensing, 39:8, 2255-2293, DOI: 10.1080/01431161.2017.1420938

To link to this article: https://doi.org/10.1080/01431161.2017.1420938

INTERNATIONAL JOURNAL OF REMOTE SENSING, 2018
VOL. 39, NO. 8, 2255–2293
https://doi.org/10.1080/01431161.2017.1420938

Taylor & Francis
Taylor & Francis Group

REVIEW ARTICLE

SAR-based detection of flooded vegetation – a review of characteristics and approaches

Viktoriya Tsyganskaya[a,b], Sandro Martinis [b], Philip Marzahn[a] and Ralf Ludwig[a]

[a]Department of Geography, Ludwig-Maximilians-Universität München, Munich, Germany; [b]German Remote Sensing Data Center (DFD), German Aerospace Center (DLR), Wessling, Germany

ABSTRACT

The ability of synthetic aperture radar (SAR) to detect flooded vegetation (FV) (the temporary or permanent occurrence of water-bodies underneath vegetated areas) offers a great benefit in the research fields of flood and wetland monitoring. The growing demand for near real-time information in flood monitoring and an increased awareness of the importance of wetland ecosystems are strong drivers for the ongoing research in these fields, where FV constitutes an essential part. This study reviewed 128 publications summarizing the knowledge about the relationships between the SAR parameters and the environmental conditions for the detection of FV. An advanced review of 83 studies was carried out to gain insights about applied classification techniques and SAR data for the extraction of FV. Although some trends emerged about which wavelengths, polarisations, or incidence angles to use, there is variation in the application of different classification techniques or using SAR-derived information depending on the data sets and the study area. Notable throughout the analysed articles is the growing demand for unsupervised and computationally efficient methods of higher accuracy for the extraction of FV. Based on the advances in SAR with regard to spatial and temporal resolution, the development of robust approaches for the extraction of FV from various and complex environments has to be further pursued.

ARTICLE HISTORY
Received 28 March 2017
Accepted 5 December 2017

1. Introduction

Detection and extraction of flooded vegetation (FV) is of particular importance for two application fields: wetland and flood monitoring. Wetlands comprise open water areas, as well as different types of FV (e.g. emerging woody, herbaceous vegetation) (White et al. 2015), which can be permanently or seasonally flooded. Wetlands are important ecosystems providing many essential services, such as flood control, sediment storage, wildlife habitat, filtering of contaminants, recreation, aesthetic value, and others (Millennium Ecosystem Assessment 2005). Despite these benefits, wetlands have been extensively converted to agriculture areas worldwide (Asselen et al. 2013) and

CONTACT Viktoriya Tsyganskaya viktoriya.tsyganskaya@iggf.geo.uni-muenchen.de Ludwig-Maximilians-Universität München, Department of Geography, Luisenstr. 37, Munich 37, 80333, Germany

furthermore are endangered by climate change (Erwin 2009). Continuous monitoring of changes in wetlands contributes to their protection.

In comparison to wetland monitoring, detecting FV for flood monitoring is a relatively young field. Besides the detection of open waterbodies, the focus lies on the extraction of FV. The availability of detailed near real-time information about the extent of inundation areas at large scales is a significant data source for many institutions, such as humanitarian relief organizations, decision makers for crisis management or insurance companies. In contrast to open flood surfaces, there is little research on the detection of flooded areas underneath vegetation. However, the disregard of FV can lead to an underestimation of the extent of an inundation, which may lead to higher risk to human lives and damage of their properties. Furthermore, flood affects agricultural areas worldwide, entailing enormous economic losses (Trujillo 2015). These possible impacts show the importance to continue the investigations in the field of FV as a part of wetland detection and flood monitoring.

The terminology and definition of FV vary from survey to survey, depending on its scope and study area. Terms such as partially submerged vegetation (Martinis und Rieke 2015) or FV (e.g. Pierdicca et al. 2008; Pulvirenti et al. 2013; Pulvirenti et al. 2016; Martinez und Le Toan 2007; Martinis und Twele 2010) can be found in the corresponding literature. The designation FV is used to describe unspecified types of FV or as an umbrella term for different vegetation types (e.g. standing water underneath forested or in between agricultural areas) (Betbeder et al. 2014; Schlaffer et al. 2016). In the scope of this review, the term FV describes the temporary or permanent occurrence of a water surface beneath a vegetation canopy; however, it does not consider vegetation areas, which are completely covered by water. In agricultural or herbaceous areas, the leaves or stems of the plants visibly emerge above the water surface. In forests or tree stands, standing water can occur underneath the vegetation canopy during flood conditions. FV summarizes different terms related to the aforementioned definition used in the reviewed literature.

Synthetic aperture radar (SAR) is a well-known and well-established tool for the extraction of FV from space due to numerous advantages. In comparison to optical sensors, the SAR systems use longer wavelengths of the electromagnetic spectrum, allowing cloud penetration and therefore weather independent image acquisition. Furthermore, SAR systems are active sensors, transmitting and receiving their own electromagnetic impulses, which allows operations independent of daylight (Klemas 2013; Betbeder et al. 2014). A relatively high energy supply is required for SAR observations, which can be a restricting factor for the availability of SAR time series data and even for the acquisition of single images in some regions in the world. However, the recently launched C-band Sentinel-1 and L-band ALOS-2 satellite missions may now overcome this limitation and therefore provide a possibility for continuous monitoring of ground features and their changes over time with short revisit times (White et al. 2015). The main advantage of SAR technology, however, is the ability to detect FV due to its capability to penetrate the vegetation canopy to a certain extent depending on the wavelength and its sensitivity to water underneath the vegetation. SAR backscatter intensity (BI) values can significantly increase during the presence of water underneath vegetated areas due to the double- or multi-bounce interaction between the specularly reflecting water surface and vertical structures of the vegetation, such as trunks and stems (Moser et al. 2016; Pulvirenti et al. 2013; Pulvirenti et al. 2011a).

While there are clear advantages of SAR data regarding the detection of FV, there are a number of challenges regarding SAR image analysis and its interpretation, as well as limitations, particularly for FV mapping. Speckle, which is inherent to all SAR imagery, may lead to uncertainties in measurements and may consequently result in a decrease of the classification accuracy. This effect can be mitigated using spatial or temporal speckle filters (Lopes, Touzi, and Nezry 1990; Quegan und Yu 2001). Further limitations appear in hilly regions due to geometric and radiometric effects (e.g. foreshortening and layover) occurring in side-looking systems such as SAR (White et al. 2015). These effects increase with small look angles and steep slopes. A correction of these effects has to be applied to reduce their influence. Furthermore, the enhancement caused by double-bounce, as discussed before, is not always detectable depending on the environmental parameters (e.g. above-ground biomass) and sensor characteristics (e.g. wavelength). Finally, backscatter intensities of FV can be similar to the backscatter intensities of urban areas and bare soil areas with high-moisture content. This can result in confusion with FV and misclassification (Chapman et al. 2015; Pulvirenti et al. 2016). In summary, dealing with SAR data can be a challenging task; however, it also constitutes a great opportunity for the mapping of FV due to the aforementioned advantages, if the complexity of these data is well understood.

Overviews and reviews about the potential and capability of SAR systems for the detection of FV have been provided in the research fields of wetland and flood monitoring. These reports summarize the knowledge about the relationships between the sensor parameters (wavelength, polarisation, incidence angle) and environmental conditions (e.g. vegetation type, phenology of plants, soil moisture). Useful status reports have been provided by Hess, Melack, and Simonett (1990), Hall (1996), Schmullius and Evans (1997), Henderson and Lewis (2008), and Silva e al. (2008). Analysis and classification methods for the detection of FV have been summarized by Henderson and Lewis (2008). In addition, there have been more recent reviews briefly and fragmentarily discussing the detection of FV, as part of a more general overview (White et al. 2015) or in a context of a specific topic, such as object-based analysis in wetlands (Dronova 2015) or sensing of mangrove ecosystems (Kuenzer et al. 2011), emergent and submerged wetlands (Klemas 2013), and flood inundation with microwaves (Schumann und Moller 2015).

The technical progress of SAR systems and the advances in computer technology have led to an intensive effort to develop suitable algorithms for the extraction of FV from SAR imagery over the last decades. Furthermore, the growing demand for near real-time information in flood monitoring and an increased awareness of the importance of wetland ecosystems are strong drivers for ongoing research in these fields, where FV constitutes an essential part. This article aims to provide a comprehensive and current status of the possibilities regarding the detection and extraction of FV for both flood and wetland monitoring. The following objectives are addressed,

- to give an overview of sensor characteristics and environmental conditions and their effects on the SAR signal regarding the detection of FV,
- to review the current state of the art of the classification algorithms applied to various SAR data sets for the extraction of FV, and
- to demonstrate benefits and limitations of existing methods.

The article is composed of five sections. Section 2 describes the literature selection on which the analyses are based. Section 3 provides an overview of the knowledge about the relationship between SAR parameters (e.g. wavelength, polarisation, incidence angle) and environmental parameters (e.g. aboveground biomass, water level) related to FV. Section 4 addresses various SAR data sets, the specifications of the classification algorithms including their different tasks and their respective benefits and limitations. Section 5 summarizes and concludes the aforementioned findings and illustrates future trends as well as needs for improved extraction of FV.

2. Methodology

For identification of relevant publications, a combination of key terms linked to FV, their synonyms, and related terms (Table 1) were applied as structured queries for the period from 1 January 1985 to 26 July 2016 using Web of Science (http://apps.webofknowledge.com/) as a search engine. An initial gross selection of 547 results was determined after the search restriction to articles and reviews. Further selection was conducted based on the abstract of these articles. Studies were excluded where key terms were present, but that did not refer to any form of radar data application as data source alone or in combination with other information (e.g. optical data, elevation) for the analysis or/and detection of the temporal or permanent occurrence beneath vegetated areas. Studies that did not address any form of FV, e.g. studies on vegetation only or addressing open water alone, were also excluded. The resulting set of studies containing 128 articles (Appendix 1) was then used to give an overview about effects on the SAR signal by sensor characteristics (wavelength, polarisation, incidence angle), environmental parameters (e.g. aboveground biomass, soil moisture, water depth), and their interaction.

An advanced selection was performed for the identification of studies, which applied classification algorithms for the extraction of FV. Based on this search, 83 studies were determined, published in the period from 1994 to July 2016 (Table 2). This new set of articles provides an overview of the diversity of applied data sets and classification algorithms aiming at the extraction of FV. The data sets include various SAR-derived information (BI, polarimetric parameters [PPs], and interferometric coherence [IC]). Furthermore, the classification algorithms differ regarding the level of classification (pixel or segment based) and the temporal frequency of the applied SAR data, which is investigated by categorizing the studies into single date, change detection, order-independent multi-date, and time series approaches. The identified classification algorithms are categorized into various groups to demonstrate the diversity of applied methods, their number of occurrences in the studies, and their requirements for preliminary information, such as training samples (supervised or unsupervised approaches). Their benefits and limitations are

Table 1. Search key words applied to select studies for this review and the initial number of results for each combination of key words.

Key words (topics)	Number of results	Number of results (articles and reviews)
(radar OR microwave* OR SAR*) AND (flood* OR inundat*) AND ('flooded vegetation' OR forest* OR agricultur*) AND (classif* OR mapp* OR extract*)	265	186
(radar OR microwave* OR SAR*) AND wetland* AND (classif* OR mapp* OR extract*)	483	361

Table 2. Eighty-three selected SAR remote-sensing studies of FV.

Study ID	Reference	Sensor	Wavelength	Polarization	Incidence angle	PFV types	Location
1	Allen, Wang, and Gore (2013)	ALOS PALSAR	L	HH, HV	Unspecified	Wetland	Carolina, USA
2	Arnesen et al. (2013)	ALOS PALSAR	L	HH	28°–35°	Flooded forest	Brazil, South America
3	Augusteijn and Warrender (1998)	Airborne Imaging Radar SAR	C, L, P	HH, HV, HV, VV	21°–34°	Forested wetlands	Maryland, Canada
4	Baghdadi et. al. (2001)	Airborne (SAR-580) ERS-2; RADARSAT-1	C	HH, HV, HV, VV	10°–60°	Wetland	Ontario, Canada
5	Betbeder et al. (2014)	TerraSAR-X	X	HH, VV	37°	Forested wetlands	France, Europe
6	Betbeder et al. (2015)	TerraSAR-X	X	HH,VV	37°	Wetland	France, Europe
7	Bian et al. (2016)	ALOS PALSAR	L	HH, HV	Unspecified	Flooded forest	Changchun, China
8	Bourgeau-Chavez et al. (2001)	Shuttle Imaging Radar-C, ERS-1, RADARSAT-1, JERS-1, ENVISAT ASAR, RADARSAT-2	L, C	HH, HV, HV, VV	25°	Forested wetlands	Virginia, USA
9	Bourgeau-Chavez et al. (2009)	JERS-1, RADARSAT-1, ERS-1, PALSAR	L, C	HH, VV, HV	35°, 23°, 47°	Wetland, flooded forest	Greate Lakes, Canada
10	Bourgeau-Chavez et al. (2016)	ALOS PALSAR, RADARSAT-2	L, C	HH	34°, 42°, 19°, 24°	Forested wetlands	Michigan, USA
11	Bouvet and Le Toan (2011)	ENVISAT	C	HH	17°–42°	Rice paddies	Vietnam, Asian
12	Brisco et al. (2011)	Airborne (SAR-580), Simulated RADARSAT-2	C	HH, HV, HV, VV	45°–60°	Wetland	Manitoba, Canada
13	Brisco et al. (2013b)	RADARSAT-2	C	HH, HV, HV, VV	26°, 36°, 41°	Rice, Wetland	China, Asian
14	Bwangoy et al. (2010)	JERS-1	L	HH	37°	Wetland	Congo, Africa
15	Cazals et al. (2016)	Sentinel-1	C	VV, VH	36°–42°	Flooded vegetation	French, Europe
16	Chapman et al. (2015)	ALOS PALSAR	L	HH	35°	Flooded vegetation	South America
17	Chen et al. (2014)	ALOS PALSAR	L	HH, HV, VH, VV	24°	Wetland	Yancheng, China
18	Corcoran et al. (2012)	RADARSAT-2	C	HH, HV, VH, VV	26°, 28°	Wetland	Minnesota, USA
19	Cordeiro and Rossetti (2015)	ALOS PALSAR	L	HH, VH	Unspecified	Wetland	Brazil, South America
20	Costa et al. (1997)	RADARSAT-1, JERS-1	C, L	HH	Unspecified	Flooded forest	Brazil, South America
21	Costa et al. (2002)	RADARSAT-1, JERS-1	C, L	HH	43°; 35°	Flooded forest	Brazilian, South America
22	Costa (2004)	RADARSAT-1, JERS-1	C, L	HH	43°, 35°	Flooded forest	Brazil, South America
23	Costa and Telmer (2006)	RADARSAT-1, JERS-1	C, L	HH	25°, 50°, 35°	Wetland	Brazilian, South America
24	Cremon, Rossetti, Dilce, and Zani (2014)	ALOS PALSAR	L	HH, HV	37°–41°	Flooded forest	Brazil, South America
25	De Grandi et al. (2000)	ERS-1	C	VV	Unspecified	Flooded forest	Central Africa

(*Continued*)

Table 2. (Continued).

Study ID	Reference	Sensor	Wavelength	Polarization	Incidence angle	PFV types	Location
26	Dwivedi, Rao, and Bhattacharya (1999)	ERS-1	C	VV	Unspecified	Wetland	Bangladesh, Asian
27	Evans et al. (2010)	RADARSAT-2, ALOS (PALSAR)	C, L	HH, HV	18°–43°, 20°–41°	Flooded forest	Brazil, South America
28	Evans and Costa (2013)	ALOS PALSAR, RADARSAT-2, ENVISAT ASAR	L, C	HH, HV	34°–39°	Wetland	Brazil, South America
29	Evans et al. (2014)	Radarsat-2, ALOS PALSAR	C, L	HH, HV	34°	Wetland	Brazil, South America
30	Ferreira-Ferreira et al. (2015)	ALOS PALSAR	L	HH, HV	39°	Flooded vegetation	Brazil, South America
31	Frappart et al. (2005)	JERS-1	L	HH	–	Flooded forest	Brazil, South America
32	Furtado, Silva, and Novo (2016)	RADARSAT-2	C	HH, HV, HV, VV	25°, 35°, 45°	Wetland	Brazil, South America
33	Gallant et al. (2014)	RADARSAT-2	C	HH, HV, HV, VV	20°–33°	Flooded vegetation	Minnesota, USA
34	Grenier et al. (2007)	RADARSAT-1	C	HH	20°–49°	Wetland	Quebec, Canada
35	Heine, Jagdhuber, and Itzerott (2016)	TerraSAR-X	X	HH, VV	38°–42°	Flooded vegetation	Germany, Europe
36	Hess (2003)	JERS-1	L	HH	34°–43°	Flooded forest, Wetland	Brazil, South America
37	Hess et al. (2015)	JERS-1	L	HH	Unspecified	Flooded forest	Brazil, South America
38	Hidayat et al. (2012)	ALOS PALSAR	L	HH	Unspecified	Flooded forest	Indonesian, Asian
39	Karszenbaum, et al. (2000)	RADARSAT-1, ERS-2	C	HH, VV	20°–46°	Wetland	Argentina, South America
40	Li and Chen (2005)	RADARSAT-1	C	HH	45°	Wetland	Ontario, Canada
41	Lee et al. (2015)	ALOS PALSAR	L	Unspecified	Unspecified	Wetland, flooded forest	Congo, Africa
42	Long, Fatoyinbo, and Policelli (2014)	ENVISAT ASAR, RADARSAT-2	C	HH	Unspecified	Flooded vegetation	Namibia, Africa
43	Maillard, Alencar-Silva, and Clausi (2008)	RADARSAT-1	C	HH	24°–31°, 41°–46°	Flooded forest	Brazil, South America
44	Martinez and Toan (2007)	JERS-1	L	HH	34°–43°	Flooded forest	Brazil, South America
45	Martinis and Twele (2010)	TerraSAR-X	X	HH	27°–36°	Flooded shrubs and grassland	Namibia, Africa
46	Marti-Cardona et al. (2013)	ENVISAT ASAR	C	HH, VV	19°–45°	Flooded vegetation	Spain, Europe
47	Mayaux et al. (2002)	ERS, JERS-1	L, C	VV, HH	19°–26°, 37°–42°	Flooded forest	Congo, Africa
48	Melack and Wang (1998)	JERS-1	L	HH	35°	Flooded forest	Brazil, South America
49	Miranda, Fonseca, and Carr (1998)	JERS-1	L	HH	Unspecified	Flooded forest	Brazil, South America

(*Continued*)

Table 2. (Continued).

Study ID	Reference	Sensor	Wavelength	Polarization	Incidence angle	PFV types	Location
50	Morandeira et al. (2016)	RADARSAT-2	C	HH, HV, HV, VV	42°–44°, 26°–28°	Wetland	Paraguay, South America
51	Moser et al. (2016)	TerraSAR-X	X	HH, VV	27°–28°	Wetland	Burkina Faso, Africa
52	Mwita et al. (2012)	ALOS PALSAR, ENVISAT ASAR	L, C	HH, HV, HV, VV; HH, HV	Unspecified	Wetland	Kenya, Africa
53	Na et al. (2013)	ENVISAT ASAR	C	HH, HV	19°–27°	Wetland	Heilongjiang, China
54	Na et al. (2015)	RADARSAT-2	C	HH, HV	26–31°	Forested wetlands	Heilongjiang, China
55	Pierdicca et al. (2008)	ERS-1	C	VV	Unspecified	Flooded woodland and grassland	Italy, Europe
56	Pistolesi, Ni-Meister, and McDonald (2015)	ALOS PALSAR	L	HH, HV	34°	Flooded forest	New York, USA
57	Podest and Saatchi (2002)	JERS-1	L	HH	Unspecified	Flooded vegetation	Brazil, South America
58	Pope, Rey-Benayas, and Paris (1994)	AIRSAR	C, L, P	HH, HV, HV, VV	35°–50°	Wetland	Belize, Central America
59	Pope, Rejmankova, and Paris (2001)	Endeavour (SIR-C)	C, L	HH, HV, HV, VV	26°	Wetland, flooded forest	Mexico, North America
60	Pulvirenti, Pierdicca, and Chini (2010)	COSMO-SkyMed	X	HH	Unspecified	Flooded forest	Myanmar, Asian
61	Pulvirenti et al. (2011a)	COSMO-SkyMed	X	HH	26°–51°	Flooded agriculture	Italy, Europe
62	Pulvirenti et al. (2011b)	COSMO-SkyMed	X	HH	35°; 22°	Flooded agriculture, flooded forest	Albania, Europa
63	Pulvirenti et al. (2013)	COSMO-SkyMed	X	HH	29°–47°	Flooded agriculture, flooded forest	Italy, Europe
64	Pulvirenti et al. (2016)	COSMO-SkyMed	X	HH	34°, 40°	Flooded agriculture	Italy, Europe
65	Rebelo, Senay, and McCartney (2012)	ALOS PALSAR	L	HH	Unspecified	Flooded vegetation	South Sudan, Africa
66	Robertson, King, and Davies (2015)	RADARSAT-2	C	HH, HV, HV, VV	18°–48°	Wetland	Ontario, Canada
67	Rodrigues and Souza-Filho (2011)	RADARSAT-2	C	HH	20°–31°	Flooded tropical forest	Brazil, South America
68	Schlaffer et al. (2016)	ENVISAT ASAR	C	HH	15°–45°	Wetland	Zambia, Africa
69	Simard, Saatchi, and De Grandi (2000)	JERS-1	L	HH	Unspecified	Flooded tropical forests	Gabun, Africa
70	Simard et al. (2002)	JERS-1, ERS-1	L, C	HH, VV	Unspecified	Flooded vegetation	Central Africa

(*Continued*)

Table 2. (Continued).

Study ID	Reference	Sensor	Wavelength	Polarization	Incidence angle	PFV types	Location
71	Souza-Filho et al. (2011)	SAR R99B sensor of the Amazon Surveillance System	L	HH, VV, VH	45°–53°	Flooded tropical forest	Brazil, South America
72	Townsend (2001)	RADARSAT-1	C	HH	23°–44°	Flooded forest	Carolina, USA
73	Townsend (2002)	RADARSAT-1, ERS-1	C	HH, VV	23°	Flooded forest	Carolina, USA
74	Töyrä, Pietroniro, and Martz (2001)	RADARSAT-1	C	HH	24°–47°	Flooded vegetation	Alberta, Canada
75	Töyrä et al. (2002)	RADARSAT-1	C	HH	24°–46°	Flooded vegetation	Alberta, Canada
76	Voormansik et al. (2014)	TerraSAR-X, ENVISAT ASAR	X, C	HH	42°, 24°	Flooded forest	Estonia, Europe
77	Wang et al. (1998)	ERS-1	C	VV	23°	Wetland	Ontario, Canada
78	Wang (2004)	JERS-1	L	HH	Unspecified	Wetland, flooded forest	Carolina, USA
79	Ward et al. (2014)	ALOS PALSAR	L	HH, HV	Unspecified	Flooded forest	Carolina, USA
80	Westra (2010)	ENVISAT ASAR	C	HH, HV, HV, VV	19°–36°	Wetland	Cameroon, Africa
81	Whitcomb et al. (2009)	JERS-1	L	HH	35°	Wetland	Alaska, USA
82	Zhao et al. (2014)	RADARSAT-2	C	HH, HV, HV, VV	37°–39°	Flooded forest	Northern Inner Mongolia, China
83	Zhang et al. (2015)	ALOS PALSAR, ENVISAT ASAR	L, C	HH, HV	34°	Wetland	Liaoning, China

summarized to promote the identification of methodological trends in the last decades and opportunities for further research on mapping FV.

3. Effects of sensor characteristics, environmental conditions, and their interactions on the SAR signal

The representation of FV in SAR images can vary and may be difficult to interpret because of complex interactions between SAR characteristics (wavelength, geometric resolution, polarisation, incidence angle) and environmental conditions (e.g. vegetation type, phenology of plants, soil moisture, water depth) (Hess, Melack, and Simonett 1990; Schumann and Moller 2015; Melack und Hess 2010). These different parameters can strongly influence the backscatter values and affect the ability to discriminate features on the ground surface, such as FV. Therefore, it is essential to identify sensor characteristics which can provide an appropriate basis for the development of methods aimed at the extraction of FV. This section is intended to show a further overview, supplemented by current findings about the relationship of sensor characteristics and environmental conditions having a positive effect on the detection of FV.

3.1. *Wavelength*

The backscatter values for FV vary as a function, amongst others, of radar wavelength depending on the vegetation density and structure, flood conditions, and soil moisture (Lang, Townsend, and Kasischke 2008).

Generally, the longer the wavelength, the higher the capability of the SAR signal to penetrate the vegetation canopy (Wang 2002; Hess 2003). Numerous studies concluded that L-band is suited to detect inundations beneath forested canopy and should be the preferred wavelength for this purpose (Hess, Melack, and Simonett 1990; Hess 2003; Betbeder et al. 2014). Le Toan et al. (1997), and Wang (2004) remarked, however, that the capability of L-band and also of other bands to penetrate some forested areas can be reduced or are even non-existent depending on the vegetation density, the gaps between or the height of the vegetation (see Section 3.4).

In comparison to L-band, the ability of shorter wavelengths, such as C-band, or X-band, to penetrate vegetation canopy is reduced (Costa et al. 2002; Hess 2003). Although the penetration of the C-band is limited, an increase in the backscatter values for FV was exhibited, during leaf-off as well as leaf-on conditions (Lang und Kasischke 2008; Townsend 2001), in dependency of the available polarisation (Townsend 2002). Zhang et al. (2016) showed that C-band is more useful at the initial growth stages if the density of the vegetation is low. Also, C-band data has the potential to detect paddy rice cultivation (Brisco et al. 2013b; Le Toan et al. 1997) and herbaceous wetlands (Grings et al. 2008).

X-band sensors (e.g. TerraSAR-X) produce detailed information due to their high resolution within the centimetre range (Airbus Defence and Space 2016). In general, the penetration of dense canopy by X-band is limited as a result of high interference with leaves, where backscatter is dominated by volume scattering (Voormansik et al. 2014). However, Martinis and Rieke (2015) and Voormansik et al. (2014) showed the potential of X-band to identify FV for sparse vegetation or during leaf-off conditions. In

this case, the transmissivity of the canopy is increased due to gaps in the canopy or no biomass at all and the contribution of double-bounce (interaction between water and tree trunks or branches) dominates the volume scattering. Some other studies demonstrated the ability of X-band to map FV in wetlands (Moser et al. 2016), in flooded marshland (Horritt 2003), and in olive groves (Pulvirenti et al. 2013).

Bourgeau-Chavez et al. (2001) underlined the importance of multi-frequency SAR data for consistent wetland mapping. In their study, the applied wavelengths complement their capability for the discrimination of flood underneath different vegetation types. While C-band was used to discriminate herbaceous vegetation from dry upland, the L-band was found best suitable to differentiate between flooded and non-flooded forest (Hess and Melack 2003; Zhang et al. 2016). Multi-frequency SAR data were also found useful to map flooding in wetland areas by Evans et al. (2010).

3.2. *Polarisation*

Polarisation describes the orientation of the electromagnetic field vector with respect to its direction of propagation of a SAR system, which can be horizontal (H) or vertical (V) for a single channel. The signal of a SAR system can be transmitted and received, co-polarised (HH or VV), and cross-polarised (HV or VH). Some advanced SAR systems are able to transmit and receive the signal in dual-polarised mode (HH and VV, HH and HV, VV and HV) and in all levels (HH, VV, HV, and VH). Dual- and fully polarimetric sensors are able to identify different scattering mechanisms, which are characteristic for different land-cover types (Lewis, Henderson, and Holcomb 1998; White et al. 2015).

Townsend (2002), Bourgeau-Chavez et al. (2001), Karszenbaum et al. (2000), Lang and Kasischke (2008), and Sang et al. (2014) suggested the use of HH polarisation in mapping flooded forests in comparison to VV polarisation relating to the orientation of the SAR signal for single-polarised data. This is due to the fact that the contribution of double-bounce scattering from the trunk-ground interaction is smaller at VV than at HH (Wang et al. 1995). In general, HH polarisation penetrates the vegetation canopy better than VV and, when striking the water surface, it is more strongly reflected in comparison to VV polarisation (Pierdicca et al. 2013). While the co-polarised backscatter is more sensitive to the double bounce, the cross-polarised one is more sensitive to volume scattering because of its depolarising characteristics (Marti-Cardona et al. 2010). Consequently, the backscatter increase due to FV is expected to be more detectable in co-polarised than in cross-polarised data (Hess, Melack, and Simonett 1990). Nevertheless, the combination of co- and cross-polarised data may improve the identification of FV as the double bounce allows a better discrimination between different FV types (Zhao et al. 2014).

Single-polarised SAR data are able to identify FV due to an increase in backscatter values in comparison to other land-cover types. These data are often used due to its greater coverage and higher spatial resolution in comparison to dual- or quad-polarised SAR data. The source of this increase in backscatter values is assumed to be the fact that vegetation under flood conditions can act as corner reflectors causing double-bounce effects (Moser et al. 2016; Pulvirenti et al. 2013). The individual backscatter mechanisms, such as double bounce, cannot be identified in single-polarised images. However, single-polarised data, which provide BI, may increase during flood conditions (Betbeder et al. 2014). Some objects (e.g. urban structures, ploughed bare soils) may cause similar

backscatter intensities as FV. The similarity of SAR backscatter only constitutes a critical issue when analysing single-polarised images (Schumann and Moller 2015; Martinis and Rieke 2015; Pulvirenti et al. 2016). The use of ancillary data (e.g. land-cover map, optical data) may reduce the confusion between the aforementioned objects by exclusion of non-vegetated features. In the past, studies increasingly used single-polarised data for the detection of different FV types, such as forested wetlands (Bourgeau-Chavez et al. 2001; Pistolesi, Ni-Meister, and McDonald 2015), marshland (Horritt 2003), as well as agricultural areas (Pulvirenti et al. 2011b; Kasischke et al. 2003).

Single-polarised SAR data only provide BI and, according to White et al. (2015) and Betbeder et al. (2014), are not quite efficient enough to detect FV due to the restricted information content about backscatter mechanism such as the double-bounce effect. SAR systems with multi-polarised SAR data (dual-polarised and fully polarised) have significant advantages in comparison to single-polarised SAR data, providing more information about the presence of water underneath the vegetation canopy (Souza-Filho et al. 2011).

Dual-polarised SAR data are generally used to produce ratios between two polarisation types. Brisco et al. (2011) mentioned that polarisation ratios using horizontal polarisation are appropriate for mapping FV for a generalized land-cover map. Furthermore, Mougin et al. (1999) and the aforementioned study indicate the suitability of the HH/HV ratio in separating FV from uplands. According to Le Toan et al. (1997) and Wang (2004), the ratio between HH and VV is higher for FV than that of most other land-cover classes, because the vertical polarised wave is more attenuated than the horizontally polarised one. Schmitt et al. (2012) designed an approach to identify FV by applying dual-polarised (HH-VV) data to distinguish between agricultural areas and swamp forest in wetlands. A recently developed approach that enables the extraction of FV by the decomposition of dual-polarised data was presented by Moser et al. (2016). The techniques for decomposition of dual-polarised SAR data are quite young; however, according to aforementioned studies, they produced promising results (see Section 4.1.2).

More known and common is the application of quad-polarised SAR data. The quad-polarised data have smaller area coverage in comparison to single- and dual-polarised SAR data. This can represent a drawback due to an inadequate coverage of the area of interest, depending on the study task. However, the quad-polarised data allow the application of polarimetric decomposition, which separates SAR signals into different scattering mechanisms: volume, single-bounce (on specular or rough surface), and dihedral scattering (double-bounce). The volume scattering mechanism represents multiple scatterings and can be found over forested and agricultural areas, where the SAR signal is diffusely backscattered by tree crowns or vegetation canopy. In case of single-bounce scattering on specular surfaces, the most of the SAR energy is reflected away from sensor. For example, these are flat open water surfaces, which often appear dark in a SAR image (Ulaby, Fung, and Moore 1986). Double- or multi-bounce scattering occurs between a specularly reflecting water surface and vertical structures of the vegetation, such as trunks and stems (Moser et al. 2016; Pulvirenti et al. 2013; Pulvirenti et al. 2011a). This scattering mechanism represents a key component for the detection of FV using SAR data.

The identification of scattering mechanisms enables the distinction of different cover types and environmental conditions, such as flood. The most frequent application of quad-polarised SAR data and decomposition techniques for detection of FV can be

found in the field of wetland monitoring due to the capability of this data to distinguish flooded and non-flooded conditions, as well as individual FV types, such as marshes and wooded wetlands or rushes (Robertson, King, and Davies 2015; Gallant et al. 2014; Schmitt und Brisco 2013; Morandeira et al. 2016; Betbeder et al. 2014). The individual decomposition techniques and their successes for the extraction of FV are described in Section 4.1.2.

3.3. *Incidence angle*

The utility of SAR data to detect FV is significantly influenced by the incident angle. It is defined as the angle between an imaginary line perpendicular to the Earth's surface and the radar signal. Depending on the satellite sensor, the incidence angles range between 10° and 65°. Thereby, the larger incidence angles are declared as shallow and the smaller angles are termed steep. Several studies, focused on the vegetation type forest, address an appropriate incidence angle for the differentiation between flooded and non-FV (Richards, Woodgate, and Skidmore 1987; Bourgeau-Chavez et al. 2001; Lang, Townsend, and Kasischke 2008). Previous investigations indicated that steeper incidence angles are preferential for the distinction of non-flooded and flooded forest (Kandus et al. 2001; Bourgeau-Chavez et al. 2001; Hess, Melack, and Simonett 1990; Richards, Woodgate, and Skidmore 1987; Costa et al. 2002). This circumstance can be explained by the SAR signal having a shorter path through the crown layer at steeper angles. As a result, the transmissivity of the vegetation canopy for SAR energy is increased. This leads to a potential increase in interaction between the surface water on the ground and the tree trunks. Shallow incidence angle signals are more influenced by the crown layer, resulting in increased volume scattering (Lang, Townsend, and Kasischke 2008; Hess 2003; Townsend 2001; Costa et al. 2002). According to the results of Lang, Townsend, and Kasischke (2008), the ability to detect waterbodies underneath forested areas did not decline as strongly as expected with increasing incidence angles, and less than expected at steeper incidence angles, in comparison to previous findings in the literature. Lang, Townsend, and Kasischke (2008) also mentioned that the angular signatures varied between different forest types and the capability to detect flooded forest is similar during the leaf-off and leaf-on conditions.

The backscatter signature of a target in two different images, acquired under similar environmental conditions, can vary in dependency of different incidence angles of these images. Depending on the task, the changes in backscatter due to different incidence angles have to be considered. For instance, Pulvirenti et al. (2011a) applied a simplified cosine model (Ulaby und Dobson 1989) assuming that the variation of backscatter can be approximated by cosine-squared function depending on the incidence angle itself. However, the use of multi-incident angle SAR images does not necessarily constitute a drawback. The results of Kandus et al. (2001) indicated that combinations of images with different incidence angles can improve the discrimination of different FV types in wetlands. In addition, Lang, Townsend, and Kasischke (2008) pointed out the benefits of multi-incident angle imagery for monitoring flood extent under forest canopies. Henderson and Lewis (2008) remarked that dense forest canopy can be appropriately detected by the combination of L-band, HH polarisation, and low-to-moderate incidence angle imagery. However, low incident angle in C-band and HH or VV polarised data is also suitable for a sparse canopy layer.

3.4. *Environmental conditions*

Besides sensor characteristics, the backscatter signature of FV is strongly affected by the environmental conditions and their characteristics, such as vegetative biomass over the ground/water (vegetation type, phenology of plants), soil moisture, and water depth. Several theoretical microwave scattering models can be found in the literature, which describe the interaction between the SAR transmitted microwave energy and vegetation or FV on the ground (Kasischke and Bourgeau-Chavez 1997; Wang et al. 1995). Low vegetation (low/moderate stage of growth) and high vegetation (e.g. deciduous forests, coniferous forests) are often considered separately in the literature (e.g. Pulvirenti et al. 2011b), because of the different effects that vegetation structure and density have on the signal intensity.

Vegetative aboveground biomass has been found to have a great influence on the scattering of FV (Pope et al. 1997). The biomass is described in various studies as canopy or crop density (e.g. Dwivedi, Rao, and Bhattacharya 1999; Grings et al. 2008) or as a combination between leafs and stems (Kasischke et al. 2003). Le Toan et al. (1997), Pope et al. (1997), Mougin et al. (1999), Sang et al. (2014), and Yu and Satschi (2016) found that SAR backscatter is increasing as a function of biomass and they determined saturation points at which water beneath the canopy cannot be detected any longer. The saturation point can shift depending on sensor characteristics (wavelengths, incidence angle, and polarisation) and environmental parameter (e.g. aboveground biomass) (Yu und Saatchi 2016; Sang et al. 2014). Before the saturation point (lower level of biomass), the transmissivity of the microwaves radiation through the vegetation canopy is possible due to the small size and density of scattering elements. If the saturation point is reached, the volume scattering from the canopy completely superimposes the contribution of double bounce from the interaction between the water surface and vertical vegetation structure (e.g. tree trunk, stems volume) (Costa et al. 2002; Kasischke et al. 2003; Aziz und White 2003). Consequently, the phenology of plants or leaf-on/leaf-off conditions highly affect the detection of FV depending on the sensor characteristics.

Beside the aboveground biomass, the contribution of the ground is another important environmental parameter influencing the backscatter signal of FV. Kasischke et al. (2003) showed an increase in backscatter through all biomass levels as soil moisture increases, provided that the transmissivity of the biomass still exists (the saturation point is not exceeded). In case of low soil moisture, as biomass increases, there is an increase due to volume scattering from the canopy; however, there is a little or no contribution from multi-interaction scattering. When the surface is flooded, there is no contribution of energy from the ground surface and the backscatter signal is dominated by the double-bounce scattering and the volume scattering from the vegetation canopy (Kwoun und Lu 2009).

Pulvirenti et al. (2011a) investigated that the water depth fluctuations significantly influence the backscatter intensities in FV areas due to the predominance of scattering mechanisms for agricultural and herbaceous vegetation. Depending on the height of the vegetation and the water depth, the double-bounce scattering can become a predominant effect and cause the increase in backscatter, while the volume scattering becomes subordinate (Bourgeau-Chavez et al. 2001; Bourgeau-Chavez, Kasischke, and Smith 1997; Grings et al. 2006; Kiage et al. 2005; Sang et al. 2014). If the emerging part of the plants

becomes too small, no considerable double-bounce scattering can be produced and the backscatter would not increase (Pulvirenti et al. 2011a). Consequently, the combination of sensor parameters and the knowledge concerning environmental properties and conditions is a crucial point for the extraction of FV.

4. Overview of methods and their data sets for the extraction of FV

Based on 83 selected studies, an overview of the diversity of applied data sets and classification algorithms aiming at the extraction of FV is given in this section. Furthermore, the classification algorithms are categorized and analysed based on the level of classification (pixel- or segment-based) and the temporal frequency of the applied SAR data. A list of the studies is provided in Table 2. Each of these studies includes a unique ID, which serves as a reference within this section.

4.1. *SAR-derived information for image classification*

For the extraction of FV various SAR-derived image, information were used in the studies comprising BI, PPs as well as IC. The number of occurrences of the SAR-derived information in the analysed studies is demonstrated in Figure 1.

4.1.1. *Backscatter intensity*

The BI for each pixel in a SAR image represents the basic SAR-derived information and the proportion of the SAR signal backscattered from the objects on the ground, depending on sensor characteristics (polarisation, frequency, incidence angle, and resolution) and environmental conditions of a target (e.g. size, shape, orientation, and moisture content). The BI values are often converted to a normalized radar cross section or backscattering coefficient, which is measured in decibel (dB) units (Henderson und Lewis 2008). Figure 1 shows that the majority of studies (69 of 83) used BI for the classifications of FV vegetation (ID 1–12, 14–16, 19–31, 34, 36–49, 52–63, 65, 67–81).

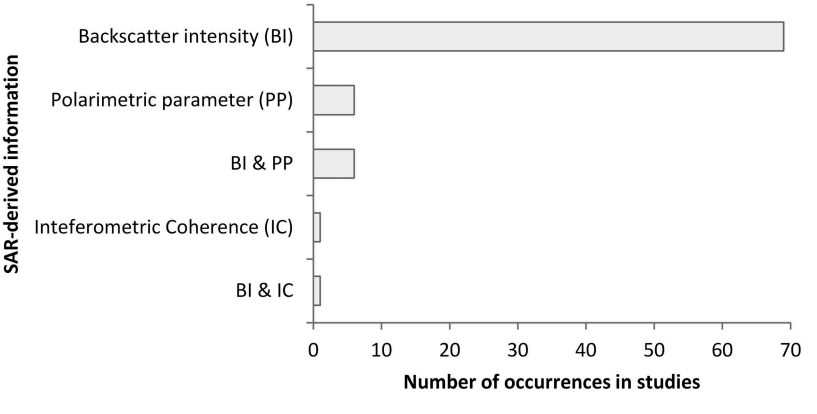

Figure 1. SAR-related information on which classifications were conducted and their number of occurrences for the extraction of FV in the selected studies.

4.1.2. *Polarimetric parameters*

The advancement of satellite systems in the recent years enables the acquisition of fully polarimetric data, transmitting and receiving the SAR signal in all four planes (HH, VV, HV, and VH). By preserving the phase information, the fully polarimetric data allow the decomposition of the SAR signal into the following three scattering mechanisms: single bounce (on specular or rough surface), volume and dihedral scattering (double-bounce) (see Section 3.2). The scattering mechanisms represent an example of PP, which are applied as extended SAR-derived information for the detection of FV. The identification of scattering mechanisms constitutes a great benefit for the extraction of FV in contrast to the single usage of BI. FV does not always have a clear BI signal that can be easily detected. For example high soil moisture conditions can cause similar backscatter values as FV. A significant challenge to differentiate both of these targets arises in the case of the application of BI on its own. The usage of PP can overcome this lack of information by providing different scattering mechanisms and consequently making it easier to separate FV types from upland areas (White et al. 2014; Heine, Jagdhuber, and Itzerott 2016) (Martinez and Le Toan 2007; Pulvirenti et al. 2011a; Pulvirenti et al. 2016; Wang und Davis 1997).

For the extraction of PP, various polarimetric decomposition methods have been developed. Usually, the polarimetric decompositions apply fully polarimetric SAR data (quad-pol data) for the extraction of FV. For the separation between FV and other areas, various decompositions (model-based and eigenvalue-based) were applied during the studies. Examples for model-based decompositions are the Freeman–Durden decomposition (ID 13, 18, 32, 33) and the Yamaguchi four-component decomposition (ID 17, 32, 82). These physically based models decompose the backscatter response from each pixel into three scattering mechanisms: volume scattering, double-bounce scattering (diplane scattering), and surface or single-bounce scattering using a Freeman–Durden decomposition (Brisco et al. 2011; Corcoran et al. 2012; Furtado, Silva, and Novo 2016; Gallant et al. 2014) and an additional fourth component (helical scattering) using the Yamaguchi four-component decomposition (Koch et al. 2012; Chen et al. 2014; Furtado, Silva, and Novo 2016; Zhao et al. 2014; Lee und Pottier 2009). One disadvantage of these models is the assumption of the objects symmetry, although most objects on the ground do not follow symmetrical orientation in consequence of their structure (Brisco et al. 2013b). However, these decompositions can be used to detect FV as two potentially perpendicular planes which act as a corner reflector in the presence of water (double-bounce scattering). The decomposition of the SAR signal into three- or four-channel images allows an easy comparison of the outputs.

An example for a decomposition based on eigenvectors is the Cloude–Pottier decomposition (Brisco et al. 2011; Chen et al. 2014; Corcoran et al. 2012; Zhao et al. 2014), which is used by further six studies (ID 13, 17, 18, 35, 50, 82). A further eigenvector-based decomposition for the derivation of PP is the Touzi incoherent decomposition (Touzi, Deschamps, and Rother 2007, 2009; Furtado, Silva, and Novo 2016; Patel, Srivastava, and Navalgund 2009), which is applied in three studies (ID 13, 17, 32). The eigenvalue-based decompositions use a coherency matrix to obtain eigenvectors and eigenvalues. Thereby, the physical scattering mechanisms are characterized by the eigenvectors and their strength (degree of randomness) is quantified by the eigenvalues (Cloude und Pottier 1997). PPs are important as they are often specific to one scattering type and

thus improve the classification of specific classes, such as FV (Heine, Jagdhuber, and Itzerott 2016).

The most common polarimetric decompositions can only be derived from fully polarised (quad-polarised) SAR data. However, the availability of quad-pol data is more limited (Moser et al. 2016; Schmitt et al. 2012). There are few decomposition approaches applicable for quad- and dual-polarised data. One of them is the method of normalized Kennaugh elements, which is adapted for any wavelength (Moser et al. 2016; Schmitt, Wendleder, and Hinz 2015) and also for all SAR sensors (ID 51). By retaining the phase information of dual-polarised data, the Kennaugh elements enable the interpretation of physical surface and double-bounce scattering mechanisms (Schmitt et al. 2012). In addition, the Shannon entropy (SE), which represents an eigenvector decomposition (Lee and Pottier 2009), can cope with dual-polarised data, too (ID 5, 6).

The compact polarimetric (CP) SAR system is configured to transmit only one polarisation, while two linear polarisations, horizontal and vertical, are received. This technique enables the creation of pseudo quad-pol data from a dual-polarised SAR system (Brisco et al. 2013b; Dabboor et al. 2015; Nord et al. 2009). An important requirement of CP is the maintenance of the relative phase between two received polarisations, which is necessary to construct CP images. The reason for the application of CP are the benefits of quad-pol data, such as improved classification through increased information content, while its drawbacks, such as reduced area coverage, are being avoided (Brisco et al. 2013b). Within this technique, m-delta decomposition is a suitable method to decompose the CP data. It is comparable to the Freeman–Durden decomposition. The simulated CP was investigated by Brisco et al. (2013b) using the m-delta decomposition for FV classification in wetland areas (ID 8).

Decompositions allow the extraction of physical information (backscatter mechanisms), but they do not represent a classification approach on their own. In the literature, the classification of decompositions for FV was mostly performed by machine-learning techniques (e.g. Support Vector Machine (ID 5, 6, 13), random forest classification (ID 18, 32, 35, 66, 82)), followed by distance-based classification methods (e.g. maximum likelihood classification (ID 13, 51), *k*-nearest-neighbour classification (KNNC) (ID 5, 17). However, also a few decision tree classifiers (ID 5, 17), two Wishard classifications (ID 17, 50), a single manual thresholding approach (MTA) (ID 33), and a single ISODATA clustering technique (ID 59) were performed based on decomposed SAR data.

Only, 12 studies performed a classification applying PP (ID 5, 6, 13, 17, 18, 32, 33, 35, 50, 51, 66, 82) (Figure 1). Several reasons for this uneven distribution can be assumed: (1) The application of PP requires dual- or quad-polarised data, in which the phase information is maintained. The advance in satellite systems during the last couple of years enables the extraction and application of the polarimetric information. (2) Based on different SAR sensors, the advanced polarisation modes might not always be available. In comparison to single-polarised data, reduced area coverage and resolution limit the usage of dual- or quad-polarised data. As a consequence, the application of polarimetric analysis for FV is restricted in comparison to the usage of BI values. (3) The preprocessing effort for BI is significantly lower in comparison to the derivation of PP (Betbeder et al. 2014; Morandeira et al. 2016; Robertson, King, and Davies 2015). (4) The interpretation of PP is likely to be more time consuming (e. g. interpretation of Pauli-Decomposition).

Figure 1 shows that exclusively PPs were applied in six different studies (ID 6, 13, 17, 18, 33, 50). Seven further studies used BI along with PP (ID 5, 32, 35, 51, 59, 66, 82). Thereby, the latter is used either as supplementary information to achieve higher accuracy for FV or as a comparison to BI-based results. Some of these studies performed comparisons of the accuracies for FV, which are described in the following. The application of BI only (HH, VV, HH/VV) resulted in poor kappa values (0.48, 0.33, 0.13) as reported by Betbeder et al. (2014). An improvement was reached using SE (kappa: 0.85) showing an accuracy of 90% PA (producer's accuracy) and 75% UA (user's accuracy) for FV. Furtado, Silva, and Novo (2016) reported that flooded forest had a 30–40% increase in PA and UA when polarimetric descriptors were used instead of only BI. The highest accuracy, therefore, is situated at 79% PA and 95% UA. Moser et al. (2016) demonstrated an increase in the PA (90%) and UA (90%) accuracy for FV extracted by PPs in comparison to the PA (79%) und UA (87%) based on BI. In addition, Robertson et al. (2016) applied BI and Cloude–Pottier decomposition for the extraction of FV showing that the UA (83%) and PA (67%) based on the BI are similar to the PA (80%) and UA (68%) based on Cloude–Pottier results. Overall, the application of PP constitutes an improvement of the accuracy for FV in comparison to results only achieved by using BI.

4.1.3. *Interferometric coherence*

A useful technique for the identification of FV constitutes the SAR interferometry through the usage of the IC, computable from two interferometric SAR images. The application of interferometric SAR technology is relatively new in the research field of the extraction of FV and limited based on several requirements of certain conditions, such as maintained phase information in the SAR data or a short temporal baseline between an interferometric pair (Pulvirenti et al. 2016). Recently published studies used IC information alone (ID 83) and in combination with the BI (ID 64) for the extraction of FV (Figure 1). The coherence might help differentiating between vegetation and bare soil areas, where the latter has considerably higher coherency values. Consequently, the coherence may replace the application of ancillary information, such as optical data or land-cover information, which is often used to separate between various objects with similar BI. The combination of both, BI values and associated phase coherence, enables the discrimination of non-flooded and FV (Alsdorf et al. 2000; Alsdorf, Smith, and Melack 2001; Kwoun and Zhong 2009; Oliver-Cabrera und Wdowinski 2016; Xie et al. 2013; Zhang et al. 2015).

4.2. *Specification and comparison of applied classification techniques*

Based on 83 studies, a comprehensive review of the classification techniques applied for the extraction of FV was conducted. The algorithms are placed in categories, due to their similarity towards each other and in regard to their application fields. Thereby, the number of the applied approaches can exceed the number of the analysed studies as a single study can implement more than one of these approaches (overall 101 classification algorithms in 83 studies).

These classification techniques can be categorized into supervised and unsupervised classification techniques (Figure 2). In general, supervised classification uses reference

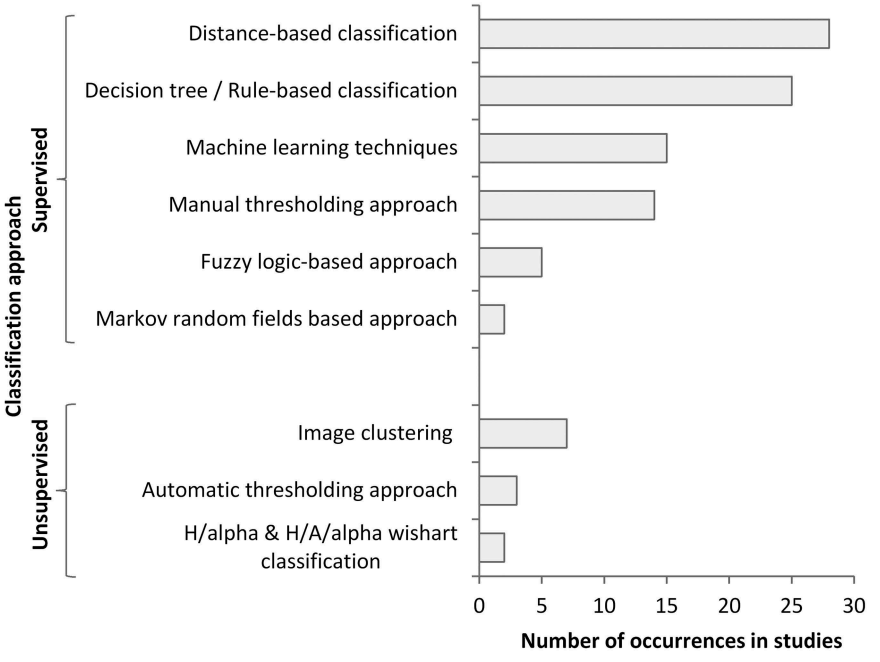

Figure 2. Supervised and unsupervised classification techniques and their number of occurrences for the extraction of FV in the selected studies.

classes obtained from training samples (reference data) to classify the image elements (Richards 2012). The majority of the performed classification algorithms in each study are supervised (89 studies). The number of occurrences of unsupervised techniques for the extraction of FV in the studies is comparatively low (12 studies). Furthermore, unsupervised classification algorithms are mostly applied as a part of a processing chain, which additionally includes a supervised classification algorithm or manual interaction steps.

The range of classification algorithms applied for the extraction of FV is diverse (Figure 2). The distance-based classification methods constitute the majority of the applied classification algorithms amongst the analysed studies (28 of 83). Whereby, algorithms are categorized as distance-based because they are using simple distance functions. Figure 3 shows the number of occurrences for distance-based classifications. Maximum likelihood classification (MLC) was identified as one of the most common classification techniques within the distance-based methods (15 of 29) applied for the extraction of FV (ID 8, 9, 12, 13, 23, 25, 49, 51, 53, 56, 57, 67, 71, 77, 80). The supervised KNNC was applied four times for the extraction of FV (ID 5, 17, 54, 80). A parallelepiped classification is one of the distance-based classification methods and was used in three studies (ID 26, 44, 49). Three of the distance-based classifications used the Mahalanobis distance (ID 43, 74, 75). Other two studies applied the Bhattacharyya distance (ID 20, 21, 22). Due to their simplicity, availability, and statistical transparency (no black box), these algorithms are popular tools not only for classification in general but also for detecting FV. Furthermore, they can be easily adapted to other study sites or data sets (Martinez and Le Toan 2007). Especially MLC and KNNC are often used as a reference for the performance of newly developed algorithms (Bourgeau-Chavez et al. 2001; Brisco et al.

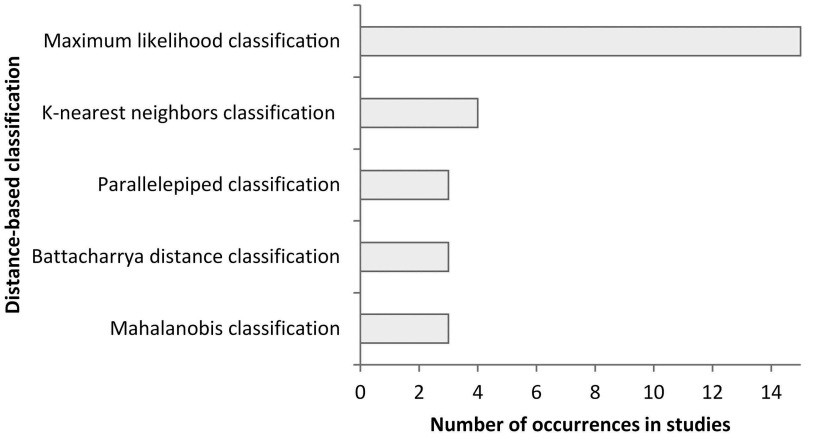

Figure 3. Categorization of distance-based classifications and their number of occurrences for the extraction of FV in the selected studies.

2013b). However, Na et al. (2015) remarked that MLC and KNNC are in general not suitable for the analysis of high dimensional data, which can constitute a drawback for the extraction of FV.

The second most common approach used in the reviewed studies (25 of 83) is the decision tree/rule-based classification (Figure 2), which includes decision tree classification (DTC) and hierarchical rule-based classification (HRBC).

Figure 4 shows the number of occurrences of both approaches, where the majority of studies (20) applied DTC for the extraction of FV (ID 2, 4, 5, 7, 9, 14, 17, 19, 40, 42, 44, 48, 52, 60, 69, 70, 72, 73, 78, 79). A decision tree classifier is well adapted for SAR image classification, because it does not assume a special probability density distribution of the given input data (Baghdadi et al. 2001; Hess et al. 1995). This algorithm is based on hierarchical rules representing thresholds used to iteratively split data in more homogeneous groups (Richards 2012), which can be easily refined after iterations (Martinez and Le Toan 2007). The automatic boundary definition constitutes an advantage because manually determining thresholds, especially for separation of FV to other classes, can be a complex process. A further advantage of decision trees is their flexibility and robustness regarding nonlinear and noisy relations among input features (Townsend 2002; Friedl und Brodley 1997; Na et al. 2015). This is a benefit for the detection of FV, because of the

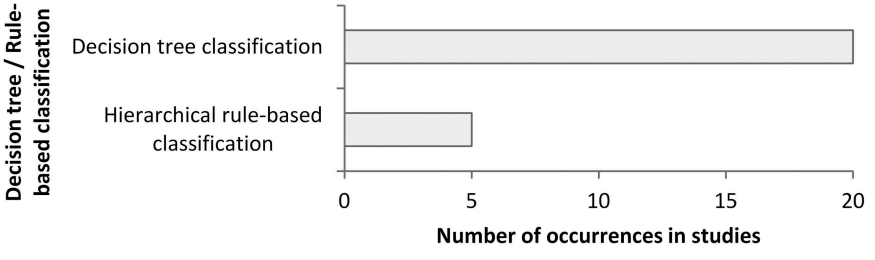

Figure 4. Decision tree and hierarchical rule-based classifications and their number of occurrences for the extraction of FV in the selected studies.

diversity of the applied input data for its extraction. Additionally, DTC requires less time for training in comparison to machine-learning algorithms (e.g. artificial neural networks [ANNs], Support Vector Machine) (Na et al. 2015).

Three studies used the HRBC for the extraction of FV (ID 27, 28, 29, 37, 47), in which the classification rules are designed by users based on their knowledge and expertise and can be iteratively changed depending on the results of the classification process. Therefore, specific characteristics of FV can be systematically integrated into the rule set. The transparency of this approach ensures that this knowledge can be used as basis for further studies and decisions. Furthermore, HRBC allows adding new rules or data sets without altering the predefined rules, while distance-based methods, such as MLC, may change all classes' rules due to additionally added information (Evans et al. 2010).

Several studies (15 of 83) used machine-learning techniques for the extraction of FV (Figure 2). Figure 5 shows various machine-learning techniques which were applied in the reviewed studies and their number of occurrences.

The majority of these techniques (11 of 15) is represented by the Random forest classification (RFC) (ID 10, 18, 24, 32, 35, 46, 53, 54, 66, 81, 82). RFC is an ensemble classifier containing multiple decision trees and consequently, the aforementioned advantages of DTC also shared by RFC. By averaging multiple decision trees, the usual overfitting of each decision tree can be reduced (Richards 2012). This algorithm efficiently determines the contribution of diverse information to a classification. However, the application of different information types without the understanding of the true relations within this information can also constitute a disadvantage. For instance, SAR data can be rated less important due to a better correlation of optical data with other features for the extraction of FV. In this particular case, RDF may ignore the context and set the priority to the highest correlated data. Furthermore, a large set of reference data is needed to mitigate misclassification caused by natural variability within FV (Robertson, King, and Davies 2015).

Support Vector Machine (SVM) classification, which is used in three studies (ID 5, 6, 13), aims to separate two different classes by determining the maximum-margin hyperplanes for a given training set. SVMs are intended for the determination of the best linear separation between two categories within a new feature space. Moreover, the SVM classification is suitable for high-dimensional data even though limited training data are available (Richards 2012), which is often the case when working with FV.

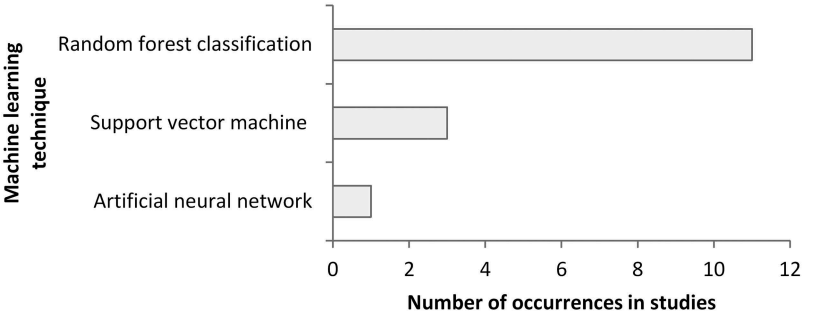

Figure 5. Machine-learning techniques and their number of occurrences for the extraction of FV in the selected studies.

A single study (ID 3) applied ANNs. This machine-learning algorithm is inspired by the neural structure of the human brain (Richards 2012). A huge disadvantage of this method is the fact that a large sample set is required to provide an effective training of the model. This in return could result in a high computation time. Nevertheless, ANN has demonstrated several advantages for image classification. Various heterogeneous data sources (e.g. temperature, SAR intensities, soil moisture level) can be combined as input. In addition, the algorithm works without any assumption about the distribution of the data (Augusteijn und Warrender 1998). As discussed above, both advantages are beneficial for the extraction of FV.

A fuzzy logic-based approach was applied in five studies (ID 34, 45, 55, 62, 63) to deal with the ambiguities of the SAR signature and to integrate different sources of information, such as SAR BI, elevation distance to open flood areas, and neighbourhood relationships between pixels. This constitutes an advantage regarding the extraction of FV. In classical set theory, an element may or may not belong to a set, as against in a fuzzy set, where all elements have different degrees of membership (Buckley und Eslami 2002). The selection of an appropriate membership function to build up a fuzzy set is subjective and it depends on the task and the available data. It can be challenging to locate FV in transition zones between open water and upland in SAR images due to their variations over the time (Wang 2004). Fuzzy logic has the ability to overcome these uncertainties by describing the increase of backscatter induced by FV using membership functions without crisp thresholds.

Another supervised method for the extraction of FV is the MTA used in 13 studies (ID 11, 15, 16, 30, 31, 33, 38, 39, 41, 64, 65, 76, 83). Defining the threshold value is a crucial point as environmental and sensor parameters show strong mutual dependencies. The threshold for FV has to be individually determined for each study area and is therefore non-transferable towards other regions. However, this method provides the ability to separate between FV and other classes quickly and without much effort, for example using histogram thresholding (ID 42, 76).

In contrast, Otsu's (Otsu 1979) and Kittler and Illingworth's (Kittler und Illingworth 1986) thresholding methods represent unsupervised classification techniques which automatically perform histogram shape-based thresholding (ID 45, 62, 63). A fast classification of clearly separable classes and therefore the creation of a quick overview of the existing classes are great benefits of automatic thresholding techniques. However, the separation between FV and non-FV is challenging due to the wide range of values within both categories that may lead to overlapping histograms. Therefore, the automatic thresholding technique is usually only applied as part of a processing chain for the extraction of FV.

Markov random fields (MRFs) are commonly used as part of an image classification processes and include various types of contextual information (e.g. spatial, hierarchical, and temporal). The knowledge about the dependencies between neighboured pixels reveals the connections within the data providing a more appropriate basis for image classification in contrast to the consideration of isolated pixels (Li 2001). This helps to overcome challenges regarding the heterogeneity and phenological changes within FV classes. Martinis and Twele (2010) and Maillard, Alencar-Silva, and Clausi (2008) adapted MRFs within a process chain for the classification of FV among other classes (ID 43, 45).

Amongst the vast number of classification approaches to extract FV from SAR data, image clustering was used in seven studies (ID 1, 36, 52, 58, 59, 61, 68). The number of occurrences of different image clustering techniques in the reviewed studies is demonstrated in Figure 6. Image clustering is used to identify relationships within the data without any previous information (trainings sets) by dividing image elements into groups containing same or similar properties (spatial and/or temporal). Image clustering leads to a reduction of the elements to be studied and therefore provides an appropriate basis for further analysis. Furthermore, grouping of elements constitutes an advantage for the extraction of FV by means of SAR data, because speckle noise can be compensated and variation within FV as well as phenological changes can be considered.

k-Means (ID 61), *k*-medoids (ID 68), and ISODATA (ID 1, 52, 58, 59) are iterative, non-hierarchical clustering techniques of similar design. While *k*-means uses centroids for the determination of cluster centres, *k*-medoids uses medoids, which makes this algorithm more stable towards outliers. Both algorithms calculate a predefined number of clusters, even though fewer clusters might describe the data more accurately (Park und Jun 2009; Richards 2012). This disadvantage is overcome by ISODATA, which automatically merges similar clusters and splits clusters with large standard deviation during the iteration process. An iterative clustering algorithm based on the Mahalanobis distance was performed by Hess (2003) for the extraction of flooded forest and wetland types (ID 36).

Wishart H/α and H/A/α unsupervised classifications were performed by two studies (ID 17, 50). These algorithms, especially designed for decomposed SAR data, require PP, which can be obtained by decomposition (see Section 4.1.2) of dual- or quad-polarised SAR data. Morandeira et al. (2016) applied these classifications to increase expertise on the backscatter response of herbaceous wetlands (ID 50).

A few studies provided a comparison of the accuracies of the results for different classification approaches, which were implemented based on the same constellation of data sets for each study. In order to give an idea of the range of performance statistics and to demonstrate the accuracies for various algorithms, the corresponding accuracies are summarized in the following. Chen et al. (2014) compared the accuracies of the results for wetland vegetation of three different classification approaches: Wishard

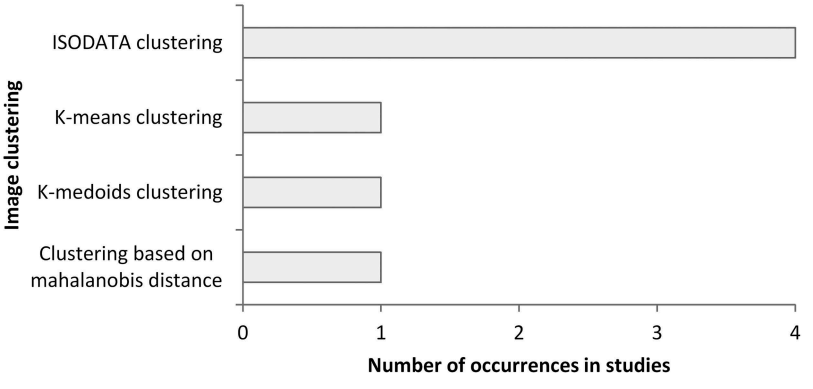

Figure 6. Image clustering techniques and their number of occurrences for the extraction of FV in the selected studies.

classification (PA: 95%, UA: 73%), KNNC (PA: 94%, UA: 78%), DTC (PA: 94%, UA: 80%). Whereby, DTC results in slightly better UA and similar or slightly worse PA compared to both others. Betbeder et al. (2014) used only the kappa index to indicate the accuracy for a study side including FV with different classification algorithm (KNNC: 0.74, DTC: 0.66, SVM using a Gaussian kernel: 0.85). The UA: 75%, PA: 90%, OA: 85% for FV were only demonstrated for SVM classifier. Na et al. (2015) showed that the results of forested and herbaceous wetlands extracted by RFC (UA: 81%, PA: 83%) outperform the results of KNNC (UA: 65%, PA: 35%).

4.3. *Pixel- and segment-based image classifications*

The classification techniques can be categorized in pixel- and segment based. In the traditional pixel-based method, each pixel of an image is classified separately, disregarding any neighbourhood relationships. By contrast, the segment-based image classification approach uses segmentation techniques to group the pixels according to their properties, such as spectral values, grey scales, texture features, or other characteristics (Mishra et al. 2016). Thereafter, the resulting segments can be classified into different land-cover features depending on the task.

Although the pixel-based approach is the most commonly used method for the extraction of FV, it may not be suitable to map heterogeneous features, such as FV, if the spatial resolution of the SAR data is finer than the objects on the ground. In this case, textural features can provide information corresponding more to FV objects and result in higher classification accuracy (Pulvirenti et al. 2011a). In contrast to pixel-based approaches, segments constitute an intuitive depiction of physical objects on the ground and allow the identification of semantic relationships. The identification of segments or regions of similar backscatter values enables these approaches to overcome the speckle noise (Hess 2003; Pulvirenti et al. 2011a). Segments are characterized by their spectral values or grey values, texture, shape, size, their neighbourhood relations, and other properties. For the extraction of FV, the texture is the most often used feature to perform a segmentation of image elements. The texture features enhance angular structures (e.g. edges) and provide information about the surfaces heterogeneity (Mishra et al. 2016). Different data sources can be combined by segments rather than by pixels due to their independence of spatial or spectral resolution (Evans et al. 2010).

In the literature, several segmentation techniques were applied to group the image elements for the extraction of FV. One of the well-known and commonly used segmentation techniques is the multiresolution segmentation. The pairwise comparison of pixel neighbours aims to minimize the heterogeneity of the resulting objects. The segmentation parameters of multiresolution segmentation have to be defined by the user, based on their knowledge and expertise, depending on the specific task. However, there is no consistent method to define the most appropriate segmentation parameter. Therefore, empirical investigations based on previous studies is necessary (Na et al. 2015; Robertson, King, and Davies 2015). Further techniques, such as Mallat's discrete wavelet transform (ID 69, 70) or Markov Random Fields (ID 43, 45), were used as a segmentation step. Commonly, the segmentation step is followed by the classification of the obtained segments applying a DTC (ID 2, 17, 19, 52, 69, 79) or a hierarchical rule-based approach (ID 27, 28, 29, 37).

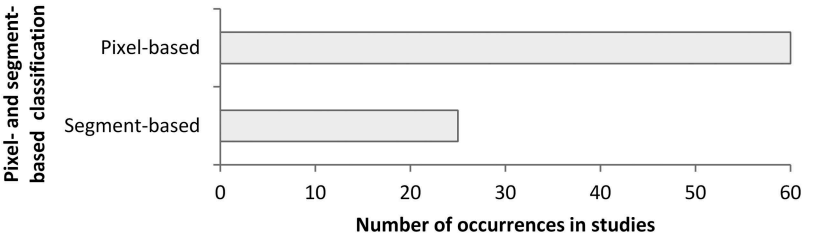

Figure 7. Pixel- and segment-based classification techniques and their number of occurrences for the extraction of FV in the selected studies.

Figure 7 shows the distribution of studies using either pixel- or segment-based classification. The majority of studies (58 of 83) applied the classification at the pixel-based scale (ID 1, 2–16, 18, 23–26, 31, 33, 35, 36, 38–42, 44, 47–51, 53–56, 58–60, 62, 64, 65, 67, 68, 70–83). The segment-based classification was performed in 23 studies (ID 2, 17, 19–22, 27–30, 32, 34, 37, 43, 45, 46, 52, 57, 61, 63, 66, 69, 79).

Three of these studies used both, pixel and segment level, to provide a comparison between the classification accuracy of the classification results (ID 17, 54, 80). A slight increase in the accuracy for FV in wetland areas was shown by Chen et al. (2014), by the application of an object-based approach (UA: 94%, PA: 81%) in comparison to a pixel-based approach (UA: 92%, PA: 77%). Na et al. (2015) demonstrated that the object-based classification (UA: 81%, PA: 83%) exceeds the pixel-based classification (UA: 67%, PA: 67%) for FV with the corresponding kappa index increasing from 0.7 to 0.8 (ID 54). Westra et al. (2010) presented the comparison between kappa values for pixel- (0.86) and for segment-based (0.83) approaches, which were carried out with different classification algorithms (MLC and KNNC). This may be the explanation for a decrease in kappa, which might not be affected by the application of pixel- and segment-based approaches. Therefore, these results are not comparable. Overall, the presumption can be made that the trend is towards segment-based approaches due to their higher accuracies.

4.4. *Approaches depending on the number of applied images in combination with SAR-derived information*

For the detection of FV, the aforementioned algorithms were applied on SAR data sets with a different number of images. Depending on the available number of SAR images, the selected studies can be categorized into four different approaches: single date, change detection, order-independent multi-date, and time-series approach (Figure 8), where more than one approach can occur in a single study. Furthermore, each category contains different SAR-derived information (BI, PP, and IC or their combination) (Section 4.3). There is a huge difference in the amount of the studies that performed a single date approach in comparison to those that performed multi-date approaches (change detection, order-independent multi-date, and time-series approach) using more than one image (52 *vs* 14, 52 *vs* 11, 52 *vs* six studies, respectively).

For the detection of FV, the single-date approach is a common method, in which the information of only one image for a current situation on the ground is considered. Despite these restrictions, the single-date approach is applied in 52 studies (ID 2–4, 12–14, 16, 17,

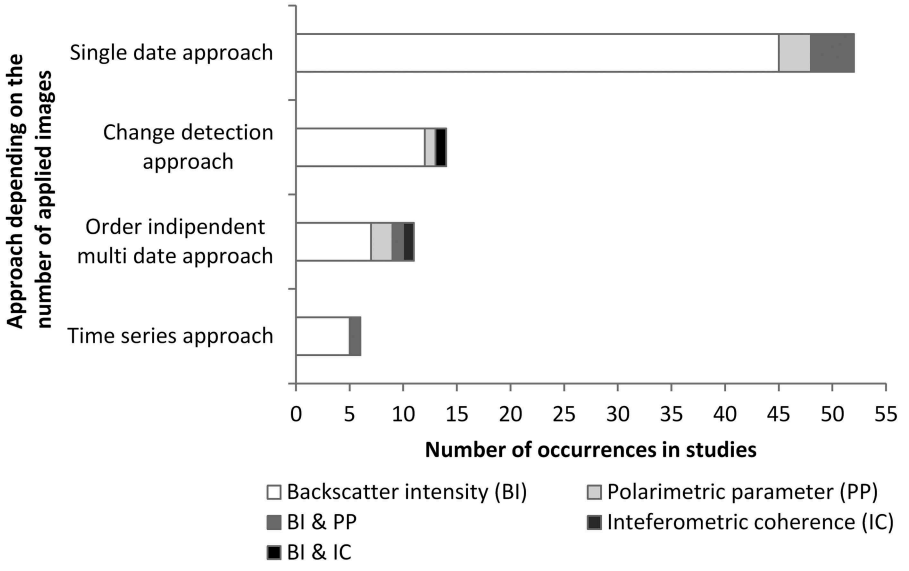

Figure 8. Summary of temporal frequency-related approaches combined with SAR-related information.

19–30, 32, 34, 35, 37, 40, 41, 43, 46, 48–50, 52–54, 56–58, 65–67, 70–76, 78–82). Land-cover maps, digital elevation models, or optical data are often used as auxiliary information to complement a single SAR date and to overcome the similarity within the BI as well as to improve the separability between FV and other classes (e.g. ID 27, 54, 72, 76). The more advanced SAR systems enable the acquisition of dual- or quad-polarised data providing extended information content in comparison to single-polarised data. In this case, ratios of the available polarisations or PP can be applied still considering only a single date. Despite this advantage, three of 52 single date approaches used PP to extract FV (ID 12, 13, 50) and four of 52 single-date approaches used both BI and PP (ID 32, 35, 66, 82). A single date only represents a snapshot of a current situations status and is therefore insufficient to detect potential changes over time.

The application of images acquired at multiple dates (two or more) may reveal the location and the extent of FV depending on the condition of their acquisition.

The reviewed studies using multiple dates can be categorized into change detection approach, order-independent multi-date approach, and time-series approach.

The change detection approach usually uses two images, acquired under dry and wet conditions, which enables to consider changes between two dates. Thereby, a change image is calculated based on the BI by the subtraction of each corresponding image element (pixel) in both images (Schumann, Di Baldassarre, and Bates 2009). The temporal change is often measured by the ratio of backscatter intensities between two dates rather than by the difference of intensities (Bouvet und Le Toan 2011). This difference between absolute backscatter intensities produces larger classification errors in regions with high backscatter than in regions with low backscatter. The ratio only depends on the relative change between two dates in SAR imagery and does not depend on the intensity level of the pixels (Rignot und van Zyl 1993). Fourteen studies demonstrated the applicability of the change detection approach for the extraction of

FV (ID 7, 10, 11, 31, 33, 39, 42, 45, 55, 60, 62, 64, 69, 77). Despite the advantage to detect changes between two images, the application of a change detection approach usually requires manual intervention for the selection of appropriate images. This selection of a scene acquired under dry conditions is critical because of the high variability in backscatter for FV depending on the environmental conditions (see Section 3.4). In addition to BI, the change detection approach was conducted based on PP (ID 33) and on the combination of BI values with IC information (ID 64).

Several studies applied multi-temporal information without the direct consideration of changes between dates in advance (ID 8, 9, 18, 36, 44, 47, 59, 83), whereby two or more acquisition dates were taken into account. In this review, these methods are summarized as order-independent multi-date approach. This approach allows the integration of different acquisition dates without knowledge about their temporal sequence. Nevertheless, it is common to integrate data from various seasons (e.g. dry and wet). Especially in the field of wetland monitoring, this approach is very popular, because different types of FV can occur during different seasons. Typical classification algorithms used in this approach are decision tree, random forest, or Support Vector Machine. Because additional information can easily be integrated, the information of PP (ID 5, 6, 18) and of IC (ID 83) were increasingly applied compared to the other three approaches discussed in this section.

The time series approach may be an appropriate solution allowing a sequential extraction of changes over time for the investigation of FV, considering seasonal or annual fluctuations of the individual vegetation types. Similar to the order-independent multi-date approach, the time series approach enables the improvement of the reliability for mapping FV areas as a consequence of multiple observations of the same area. Furthermore, the flood evolution in FV areas within an inundation event can be analysed. More details can be extracted by the shape of temporal profiles, which consider the effects of phenology and flooding and consequently enable a superior separation between FV and other classes (Betbeder et al. 2014). Overall, six studies performed the time series approach for extraction of FV. Thereby, five studies are based on BI values (ID 15, 38, 61, 63, 68); however, only one used PP as a foundation information (ID 51). Depending on the available number of SAR images, the information content can significantly increase. Martinez and Le Toan (2007) remarked that the improvement of FV accuracy depends not only on the higher number of scenes but also on the regularity of data acquisition. The complexity of analysis and processing of SAR data can considerably increase with the number of available images causing challenges in the extraction of the required information. The per-pixel analysis of backscatter time series can be CPU intensive and time consuming. In case of flood monitoring, where near real-time information is required, these characteristics may constitute a drawback. Nevertheless, several studies show benefits of the application of a time series approach. Pulvirenti et al. (2011a) demonstrated flood evolution mapping within FV by defining multi-temporal FV classes containing different stages of flood duration. Thereby, the definition of the classes was performed using multi-temporal profiles. For the extraction of the dynamics of FV, Moser et al. (2016) performed a multi-temporal classification on a stack of time-series data. Hidayat et al. (2012) calculated range, mean change, and standard deviation images using the temporal information from 20 SAR scenes. Schlaffer et al. (2016) recently introduced a harmonic model approach suitable for ENVISAT (Environmental Satellite) ASAR (advanced SAR) time-series data. This approach is

appropriate for modelling seasonal backscatter value patterns induced by different dynamics in wetlands, among others the flood evolution in vegetated areas. The harmonic model approach requires a time-series length of at least one seasonal cycle for clear classification of permanent or seasonal FV. This method represents an advanced time series approach contributing to a more automatic extraction of FV.

A comparison of the accuracy between the single image and multi-temporal approach is provided in a few of the reviewed studies and is described in the following. Wang et al. (1998) compared the accuracy of a single-date (51% correctly classified pixels) wetland classification with different combination of dates (72–85% correctly classified pixels) showing a clear improvement with higher temporal resolution. Furtado, Silva, and Novo (2016) demonstrated that the use of dual-season imagery in comparison to a single image brought the largest improvements in accuracies for flooded forest, among other classes. PA increased from 49% to 79% and UA increased from 64% to 95%, respectively. Despite the low accuracy performance reported by Heine, Jagdhuber, and Itzerott (2016), the best accuracy acquired from single-date classification (36% correctly classified proportion) was improved using multi-temporal data (45% correctly classified proportion). Zhao et al. (2014) showed that the accuracy classification of FV is improved by using multi date (PA: 97%, UA: 99%) in respect to single dates (PA: 80–92%, UA: 80–95%). Overall, an increase in accuracy using multi-date data instead of single images is reported, which can be explained by the increased information content including the seasonal stages of the plants. Thereby, the selection of specific dates constitutes the decisive factor and not necessarily their increased number Martinez and Le Toan (2007).

5. Conclusion

This review provides the current state of the art regarding the detection and extraction of FV based on 128 studies. An overview of the interaction between sensor characteristics and environmental conditions, and their effects on the SAR signal, is given. In addition, various SAR data sets and classification algorithms, as well as their benefits and limitations for the extraction of FV, are described.

As reported in earlier research reviews, longer wavelengths are still suggested for the detection of flooded forests. However, L-band and C-band can be used, both combined or individually, to separate between flooded forest, flooded herbaceous vegetation, and dry land classes. Current research also demonstrates the ability of X-band to detect FV in case of low biomass or leaf-off conditions. For the detection of FV, HH is preferred over VV and co-polarised in general over cross-polarised data. However, both are applied to discriminate between different FV types. Inhomogeneous statements were given about the application of polarisation ratios. Nevertheless, multi-polarised data were found to be valuable due to enhanced information content in comparison to single polarised data. Steeper incidence angles are still preferred over shallow ones. However, a few studies suggest that the detection of flood beneath forests with increasing incident angles is less limited than expected.

Besides sensor characteristics, the backscatter signature of FV is strongly affected by the environmental conditions and their characteristics. It was shown that the amount of the aboveground biomass is critical for the detection of FV. Therefore, saturation points of the SAR signal were determined, where the biomass increases and the water underneath the vegetation can no longer be detected. It was established that the location of the saturation

point is strongly influenced by sensor characteristics and depends on the vegetation type. Furthermore, advanced analysis of the relation between the water depth and the height of the plants has been conducted and their importance for the detection of flood in agricultural and herbaceous areas has been emphasized in several studies.

With technological advances, an increase in the variety of SAR data sets and classification algorithms has taken. BI using different polarisations is a proved basis for the extraction of FV. However, the application of PPs based on quad- or even dual-polarised SAR data leads to promising results. This is because of their increased information content and their ability to describe physical objects. Depending on the SAR data, various decomposition techniques were introduced for the extraction of PPs. In particular, the decomposition of dual-polarised data, which constitutes a compromise between information content, calculation complexity, and general availability, will provide a valuable foundation for future studies (Moser et al. 2016; Schmitt et al. 2012). IC is comparatively novel SAR-derived information which, although limited by its demanding requirements, can be beneficial as complementary information for BI (Pulvirenti et al. 2016) and reduce the need for external data (Chini et al. 2016).

The reviewed studies show some inconsistency in the application of classification algorithms used for the extraction of FV. This can be explained by the wide variety of the underlying data, which is often depending on the specific task but is mostly restricted by its availability. Thereby, the comparability of the results can be inhibited. A wide range of different classification techniques were applied in the studies, spanning from basic thresholding approaches to more complex algorithms like machine learning. A selection of a suitable algorithm for a certain task can be crucial for a successful classification and strongly depends on the applied data. With the increasing availability of data, due to a more continuous acquisition by SAR systems, such as Sentinel-1, current and prospective algorithms need to be examined in regards to their usability to extract FV. Although an increased utilization of the random forest algorithm can be noticed for wetland observations, no general trend was identified for the extraction of FV from SAR data. Even though unsupervised algorithms are applied within multiple process chains, still no completely unsupervised method exists that focuses on the extraction of FV.

The use of segmentation leads to more reliable results than pixel-based approaches, because it is less prone to speckle noise. Furthermore, segment-based approaches appear to be valuable alternatives, providing a depiction of real objects on the ground, mitigating the increasing heterogeneity of classes in high-resolution satellite imagery. Because of its potential, the segment-based approach should be more utilized for the detection of FV.

Single-image approaches are still preferred and are mostly used in combination with ancillary data, such as optical or elevation information, to describe land-cover types containing FV. The usage of multi-date SAR data sets seems to be attractive for wetland monitoring because it includes seasonal information. The comparisons between single and multi-date approaches within studies show an improvement in classification results. Short revisit times and systematic data acquisitions by satellite missions, such as Sentinel-1 (Aulard-Macler 2011) and Tandem-L (German Aerospace Center 2017), pave the way for the application of time series approaches which are already implemented, especially for flood monitoring (Schlaffer et al. 2016). Continuing efforts in the analysis of long-term profiles would expand the understanding about the seasonal and annual variability and enable the development of fully automated and potentially transferable processes for the extraction of FV.

Disclosure statement

No potential conflict of interest was reported by the authors.

ORCID

Sandro Martinis http://orcid.org/0000-0002-6400-361X

References

Airbus Defence and Space. 2016. "TerraSAR-X Documentation." Online verfügbar unter. Accessed 25 October 2017. http://www.intelligence-airbusds.com/en/228-terrasar-x-technical-documents.

Allen, T., Y. Wang, and B. Gore. 2013. "Coastal Wetland Mapping Combining Multi-Date SAR and LiDAR." *Geocarto International* 28 (7): 616–631. doi:10.1080/10106049.2013.768297.

Alsdorf, D. E., J. M. Melack, T. Dunne, L. A. K. Mertes, L. L. Hess, and L. C. Smith. 2000. "Interferometric Radar Measurements of Water Level Changes on the Amazon Flood Plain." *Nature* 404 (6774): 174–177. doi:10.1038/35004560.

Alsdorf, D. E., L. C. Smith, and J. M. Melack. 2001. "Amazon Floodplain Water Level Changes Measured with Interferometric SIR-C Radar." *IEEE Transactions Geoscience Remote Sensing* 39 (2): 423–431. doi:10.1109/36.905250.

Arnesen, A. S., T. S. F. Silva, L. L. Hess, E. M. L. M. Novo, C. M. Rudorff, B. D. Chapman, and K. C. McDonald. 2013. "Monitoring Flood Extent in the Lower Amazon River Floodplain Using ALOS/PALSAR ScanSAR Images." *Remote Sensing of Environment* 130: 51–61. doi:10.1016/j.rse.2012.10.035.

Asselen, S., P. H. Verburg, J. E. Vermaat, and J. H. Janse. 2013. "Drivers of Wetland Conversion: A Global Meta-Analysis." *PloS One* 8 (11): 1–13. doi:10.1371/journal.pone.0081292.

Augusteijn, M. F., and C. E. Warrender. 1998. "Wetland Classification Using Optical and Radar Data and Neural Network Classification." *International Journal of Remote Sensing* 19 (8): 1545–1560. doi:10.1080/014311698215342.

Aulard-Macler, M. 2011. *Sentinel-1 Product Definition, MDA Technical Note Ref. S1-RS-MDA-52–7440. MacDonald*. Richmond, Canada: Dettwiler and Associates (MDA).

Aziz, H. K., and K. White. 2003. "Using Mimics to Model L-Band SAR Mackscatter from a Peat Swamp Forest." *Journal of Tropical Forest Science* 15 (4): 546–556.

Baghdadi, N., M. Bernier, R. Gauthier, and I. Neeson. 2001. "Evaluation of C-Band SAR Data for Wetlands Mapping." *International Journal of Remote Sensing* 22 (1): 71–88. doi:10.1080/014311601750038857.

Betbeder, J., S. Rapinel, S. Corgne, E. Pottier, and L. Hubert-Moy. 2015. "TerraSAR-X Dual-Pol Time-Series for Mapping of Wetland Vegetation." *ISPRS Journal of Photogrammetry and Remote Sensing* 107: 90–98. doi:10.1016/j.isprsjprs.2015.05.001.

Betbeder, J., S. Rapinel, T. Corpetti, E. Pottier, S. Corgne, and L. Hubert-Moy. 2014. "Multitemporal Classification of TerraSAR-X Data for Wetland Vegetation Mapping." *Journal Applications Remote Sens* 8 (1): 83648. doi:10.1117/1.JRS.8.083648.

Bian, H., T. Yan, Z. Zhang, C. He, and L. Sheng. 2016. "Mapping Deciduous Broad-Leaved Forested Swamps Using ALOS/Palsar Data." *Chinese Geographic Sciences* 26 (3): 352–365. doi:10.1007/s11769-016-0805-2.

Bourgeau-Chavez, L., Y. Lee, M. Battaglia, S. Endres, Z. Laubach, and K. Scarbrough. 2016. "Identification of Woodland Vernal Pools with Seasonal Change PALSAR Data for Habitat Conservation." *Remote Sensing* 8 (6): 490. doi:10.3390/rs8060490.

Bourgeau-Chavez, L. L., E. S. Kasischke, and K. Smith. 1997. "Using Satellite Radar Imagery to Monitor Flood Conditions in Wetland Ecoystems of Southern Florida." In *Proc. SPIE 2959, Remote Sensing of Vegetation and Sea*, edited by G. Cecchi, G. D'Urso, E. T. Engman, and P. Gudmandsen, Taormina, Italy, 139–148.

Bourgeau-Chavez, L. L., E. S. Kasischke, S. M. Brunzell, J. P. Mudd, K. B. Smith, and A. L. Frick. 2001. "Analysis of Space-Borne SAR Data for Wetland Mapping in Virginia Riparian Ecosystems." *International Journal of Remote Sensing* 22 (18): 3665–3687. doi:10.1080/01431160010029174.

Bourgeau-Chavez, L. L., K. Riordan, B. Richard, N. Miller, and M. Nowels. 2009. "Improving Wetland Characterization with Multi-Sensor, Multi-Temporal SAR and Optical/Infrared Data Fusion." In *Advances in Geoscience and Remote Sensing*, edited by G. Jedlovec. Vukovar: Croatia: In-Teh.

Bouvet, A., and T. Le Toan. 2011. "Use of ENVISAT/ASAR Wide-Swath Data for Timely Rice Fields Mapping in the Mekong River Delta." *Remote Sensing of Environment* 115 (4): 1090–1101. doi:10.1016/j.rse.2010.12.014.

Brisco, B., A. Schmitt, K. Murnaghan, S. Kaya, and A. Roth. 2013a. "SAR Polarimetric Change Detection for Flooded Vegetation." *International Journal of Digital Earth* 6 (2): 103–114. doi:10.1080/17538947.2011.608813.

Brisco, B., L. Kun, B. Tedford, F. Charbonneau, S. Yun, and K. Murnaghan. 2013b. "Compact Polarimetry Assessment for Rice and Wetland Mapping." *International Journal of Remote Sensing* 34 (6): 1949–1964. doi:10.1080/01431161.2012.730156.

Brisco, B., M. Kapfer, T. Hirose, B. Tedford, and J. Liu. 2011. "Evaluation of C-Band Polarization Diversity and Polarimetry for Wetland Mapping." *Canadian Journal of Remote Sensing* 37 (1): 82–92. doi:10.5589/m11-017.

Brisco, B., R. Touzi, J. J. van der Sanden, F. Charbonneau, T. J. Pultz, and M. D'Iorio. 2008. "Water Resource Applications with RADARSAT-2? A Preview." *International Journal of Digital Earth* 1 (1): 130–147. doi:10.1080/17538940701782577.

Brown, I., S. Mwansasu, and L.-O. Westerberg. 2016. "L-Band Polarimetric Target Decomposition of Mangroves of the Rufiji Delta, Tanzania." *Remote Sensing* 8 (2): 140. doi:10.3390/rs8020140.

Buckley, J. J., and E. Eslami. 2002. *An Introduction to Fuzzy Logic and Fuzzy Sets*. Heidelberg: Physica-Verlag (Advances in soft computing).

Bwangoy, J.-R. B., M. C. Hansen, D. P. Roy, G. de Grandi, and C. O. Justice. 2010. "Wetland Mapping in the Congo Basin Using Optical and Radar Remotely Sensed Data and Derived Topographical Indices." *Remote Sensing of Environment* 114 (1): 73–86. doi:10.1016/j.rse.2009.08.004.

Cazals, C., S. Rapinel, P.-L. Frison, A. Bonis, G. Mercier, C. Mallet, S. Corgne, and J.-P. Rudant. 2016. "Mapping and Characterization of Hydrological Dynamics in a Coastal Marsh Using High Temporal Resolution Sentinel-1A Images." *Remote Sensing* 8 (7): 570. doi:10.3390/rs8070570.

Chapman, B., K. McDonald, M. Shimada, A. Rosenqvist, R. Schroeder, and L. Hess. 2015. "Mapping Regional Inundation with Spaceborne L-Band SAR." *Remote Sensing* 7 (5): 5440–5470. doi:10.3390/rs70505440.

Chen, Y., H. Xiufeng, J. Wang, and R. Xiao. 2014. "The Influence of Polarimetric Parameters and an Object-Based Approach on Land Cover Classification in Coastal Wetlands." *Remote Sensing* 6 (12): 12575–12592. doi:10.3390/rs61212575.

Chini, M., A. Papastergios, L. Pulvirenti, N. Pierdicca, P. Matgen, and I. Parcharidis. 2016. "SAR Coherence and Polarimetric Information for Improving Flood Mapping. In: 2016 IEEE International Geoscience & Remote Sensing Symposium." In *Proceedings IGARSS 2016-2016 IEEE International Geoscience and Remote Sensing Symposium. Beijing, China*, July 10-15, 2016, 7577–7580. Piscataway, NJ: IEEE.

Cloude, S. R., and E. Pottier. 1997. "An Entropy Based Classification Scheme for Land Applications of Polarimetric SAR." *IEEE Transactions Geoscience Remote Sensing* 35 (1): 68–78. doi:10.1109/36.551935.

Corcoran, J., J. Knight, B. Brisco, S. Kaya, A. Cull, and K. Murnaghan. 2012. "The Integration of Optical, Topographic, and Radar Data for Wetland Mapping in Northern Minnesota." *Canadian Journal of Remote Sensing* 37 (5): 564–582. doi:10.5589/m11-067.

Cordeiro, C. L. D. O., and D. D. F. Rossetti. 2015. "Mapping Vegetation in a Late Quaternary Landform of the Amazonian Wetlands Using Object-Based Image Analysis and Decision Tree Classification." *International Journal of Remote Sensing* 36 (13): 3397–3422. doi:10.1080/01431161.2015.1060644.

Costa, F., M. Novo, E. Mantovani, V. Ballester, and F. Ahern. 1997. "Classification of Floodplain Habitats (Lago Grande, Brazilian Amazon) with RADARSAT and JERS-1 Data." Presented ai GER'97 Conference, Ottawa, Canada, May 1997.

Costa, M. P. F. 2004. "Use of SAR Satellites for Mapping Zonation of Vegetation Communities in the Amazon Floodplain." *International Journal of Remote Sensing* 25 (10): 1817–1835. doi:10.1080/0143116031000116985.

Costa, M. P. F., and K. H. Telmer. 2006. "Utilizing SAR Imagery and Aquatic Vegetation to Map Fresh and Brackish Lakes in the Brazilian Pantanal Wetland." *Remote Sensing of Environment* 105 (3): 204–213. doi:10.1016/j.rse.2006.06.014.

Costa, M. P. F., O. Niemann, E. Novo, and F. Ahern. 2002. "Biophysical Properties and Mapping of Aquatic Vegetation during the Hydrological Cycle of the Amazon Floodplain Using JERS-1 and Radarsat." *International Journal of Remote Sensing* 23 (7): 1401–1426. doi:10.1080/01431160110092957.

Cremon, É., D. F. Rossetti, Dilce, and H. Zani. 2014. "Classification of Vegetation over a Residual Megafan Landform in the Amazonian Lowland Based on Optical and SAR Imagery." *Remote Sensing* 6 (11): 10931–10946. doi:10.3390/rs61110931.

Dabboor, M., L. White, B. Brisco, and F. Charbonneau. 2015. "Change Detection with Compact Polarimetric SAR for Monitoring Wetlands." *Canadian Journal of Remote Sensing* 41 (5): 408–417. doi:10.1080/07038992.2015.1104634.

de Grandi, G. F., P. Mayaux, J. P. Malingreau, A. Rosenqvist, S. Saatchi, and M. Simard. 2000. "New Perspectives on Global Ecosystems from Wide-Area Radar Mosaics: Flooded Forest Mapping in the Tropics." *International Journal of Remote Sensing* 21 (6–7): 1235–1249. doi:10.1080/014311600210155.

Dronova, I. 2015. "Object-Based Image Analysis in Wetland Research: A Review." *Remote Sensing* 7 (5): 6380–6413. doi:10.3390/rs70506380.

Dwivedi, R. S., B. R. M. Rao, and S. Bhattacharya. 1999. "Mapping Wetlands of the Sundaban Delta and It's Environs Using ERS-1 SAR Data." *International Journal of Remote Sensing* 20 (11): 2235–2247. doi:10.1080/014311699212227.

Erwin, K. L. 2009. "Wetlands and Global Climate Change. The Role of Wetland Restoration in a Changing World." *Wetlands Ecology Manage* 17 (1): 71–84. doi:10.1007/s11273-008-9119-1.

Evans, T. L., and M. Costa. 2013. "Landcover Classification of the Lower Nhecolândia Subregion of the Brazilian Pantanal Wetlands Using ALOS/PALSAR, RADARSAT-2 and ENVISAT/ASAR Imagery." *Remote Sensing of Environment* 128: 118–137. doi:10.1016/j.rse.2012.09.022.

Evans, T. L., M. Costa, K. Telmer, and T. S. F. Silva. 2010. "Using ALOS/PALSAR and RADARSAT-2 to Map Land Cover and Seasonal Inundation in the Brazilian Pantanal." *IEEE Journal Sel Topics Applications Earth Observations Remote Sensing* 3 (4): 560–575. doi:10.1109/JSTARS.2010.2089042.

Evans, T. L., M. Costa, W. M. Tomas, and A. R. Camilo. 2014. "Large-Scale Habitat Mapping of the Brazilian Pantanal Wetland. A Synthetic Aperture Radar Approach." *Remote Sensing of Environment* 155: 89–108. doi:10.1016/j.rse.2013.08.051.

Ferreira-Ferreira, J., T. S. F. Silva, A. S. Streher, A. G. Affonso, A. Furtado, F. de Luiz, B. R. Forsberg, et al. 2015. "Combining ALOS/PALSAR Derived Vegetation Structure and Inundation Patterns to Characterize Major Vegetation Types in the Mamirau? Sustainable Development Reserve, Central Amazon Floodplain, Brazil." *Wetlands Ecology Manage* 23 (1): 41–59. doi:10.1007/s11273-014-9359-1.

Frappart, F., F. Seyler, J.-M. Martinez, J. G. León, and A. Cazenave. 2005. "Floodplain Water Storage in the Negro River Basin Estimated from Microwave Remote Sensing of Inundation Area and Water Levels." *Remote Sensing of Environment* 99 (4): 387–399. doi:10.1016/j.rse.2005.08.016.

Friedl, M. A., and C. E. Brodley. 1997. "Decision Tree Classification of Land Cover from Remotely Sensed Data." *Remote Sensing of Environment* 61 (3): 399–409. doi:10.1016/S0034-4257(97)00049-7.

Furtado, L. F. D. A., T. S. F. Silva, and E. M. L. D. M. Novo. 2016. "Dual-Season and Full-Polarimetric C Band SAR Assessment for Vegetation Mapping in the Amazon várzea Wetlands." *Remote Sensing of Environment* 174: 212–222. doi:10.1016/j.rse.2015.12.013.

Gallant, A., S. Kaya, L. White, B. Brisco, M. Roth, W. Sadinski, and J. Rover. 2014. "Detecting Emergence, Growth, and Senescence of Wetland Vegetation with Polarimetric Synthetic Aperture Radar (SAR) Data." *Water* 6 (3): 694–722. doi:10.3390/w6030694.

German Aerospace Center. 2017. "Tandem-L. Satellite Mission Proposal for Monitoring Dynamic Processes on the Earth's Surface. Cologne. Online Verfügbar Unter." Accessed 27 August 2017. www.dlr.de/hr/en/Portaldata/32/Resources/dokumente/tdml/Tandem-L_Brochure_2017-05.pdf.

Grenier, M., A.-M. Demers, S. Labrecque, M. Benoit, R. A. Fournier, and B. Drolet. 2007. "An Object-Based Method to Map Wetland Using RADARSAT-1 and Landsat ETM Images. Test Case on Two

Sites in Quebec, Canada." *Canadian Journal of Remote Sensing* 33 (sup1): S28–S45. doi:10.5589/m07-048.

Grings, F. M., P. Ferrazzoli, H. Karszenbaum, M. Salvia, P. Kandus, J. C. Jacobo-Berlles, and P. Perna. 2008. "Model Investigation about the Potential of C Band SAR in Herbaceous Wetlands Flood Monitoring." *International Journal of Remote Sensing* 29 (17–18): 5361–5372. doi:10.1080/01431160802036409.

Grings, F. M., P. Ferrazzoli, J. C. Jacobo-Berlles, H. Karszenbaum, J. Tiffenberg, P. Pratolongo, and P. Kandus. 2006. "Monitoring Flood Condition in Marshes Using EM Models and Envisat ASAR Observations." *IEEE Transactions Geoscience Remote Sensing* 44 (4): 936–942. doi:10.1109/TGRS.2005.863482.

Hall, D. K. 1996. "Remote Sensing Applications to Hydrology; Imaging Radar." *Hydrological Sciences Journal* 41 (4): 609–624. doi:10.1080/02626669609491528.

Heine, I., T. Jagdhuber, and S. Itzerott. 2016. "Classification and Monitoring of Reed Belts Using Dual-Polarimetric TerraSAR-X Time Series." *Remote Sensing* 8 (7): 552. doi:10.3390/rs8070552.

Henderson, F. M., and A. J. Lewis. 2008. "Radar Detection of Wetland Ecosystems: A Review." *International Journal of Remote Sensing* 29 (20): 5809–5835. doi:10.1080/01431160801958405.

Hess, L. L. 2003. "Dual-Season Mapping of Wetland Inundation and Vegetation for the Central Amazon Basin." *Remote Sensing of Environment* 87 (4): 404–428. doi:10.1016/j.rse.2003.04.001.

Hess, L. L., J. M. Melack, A. G. Affonso, C. Barbosa, M. Gastil-Buhl, and E. M. L. M. Novo. 2015. "Wetlands of the Lowland Amazon Basin. Extent, Vegetative Cover, and Dual-Season Inundated Area as Mapped with JERS-1 Synthetic Aperture Radar." *Wetlands* 35 (4): 745–756. doi:10.1007/s13157-015-0666-y.

Hess, L. L., J. M. Melack, and D. S. Simonett. 1990. "Radar Detection of Flooding beneath the Forest Canopy. A Review." *International Journal of Remote Sensing* 11 (7): 1313–1325. doi:10.1080/01431169008955095.

Hess, L. L., and J. M. Melack. 2003. "Remote Sensing of Vegetation and Flooding on Magela Creek Floodplain (Northern Territory, Australia) with the SIR-C Synthetic Aperture Radar." In *Aquatic Biodiversity*, edited by K. Martens, 65–82. Dordrecht: Springer Netherlands.

Hess, L. L., J. M. Melack, S. Filoso, and Y. Wang. 1995. "Delineation of Inundated Area and Vegetation along the Amazon Floodplain with the SIR-C Synthetic Aperture Radar." *IEEE Transactions Geoscience Remote Sensing* 33 (4): 896–904. doi:10.1109/36.406675.

Hidayat, H., D. H. Hoekman, M. A. M. Vissers, and A. J. F. Hoitink. 2012. "Flood Occurrence Mapping of the Middle Mahakam Lowland Area Using Satellite Radar." *Hydrology Earth Systems Sciences* 16 (7): 1805–1816. doi:10.5194/hess-16-1805-2012.

Horritt, M. 2003. "Waterline Mapping in Flooded Vegetation from Airborne SAR Imagery." *Remote Sensing of Environment* 85 (3): 271–281. doi:10.1016/S0034-4257(03)00006-3.

Imhoff, M., M. Story, C. Vermillion, F. Khan, and F. Polcyn. 1986. "Forest Canopy Characterization and Vegetation Penetration Assessment with Space-Borne Radar." *IEEE Transactions Geoscience Remote Sensing* GE-24 (4): 535–542. doi:10.1109/TGRS.1986.289668.

Kandus, P., H. Karszenbaum, T. Pultz, G. Parmuchi, and J. Bava. 2001. "Influence of Flood Conditions and Vegetation Status on the Radar Backscatter of Wetland Ecosystems." *Canadian Journal of Remote Sensing* 27 (6): 651–662. doi:10.1080/07038992.2001.10854907.

Karszenbaum, H., P. Kandus, J. M. Martinez, T. Le Toan, J. Tiffenberg, and G. Parmuchi. 2000. *ERS-2, Radarsat SAR Backscattering Characteristics of the Parana River Delta Wetland, Argentina*. Argentina: Special Publication SP-461.

Kasischke, E. S., K. B. Smith, L. L. Bourgeau-Chavez, E. A. Romanowicz, S. Brunzell, and C. J. Richardson. 2003. "Effects of Seasonal Hydrologic Patterns in South Florida Wetlands on Radar Backscatter Measured from ERS-2 SAR Imagery." *Remote Sensing of Environment* 88 (4): 423–441. doi:10.1016/j.rse.2003.08.016.

Kasischke, E. S., and L. L. Bourgeau-Chavez. 1997. "Monitoring South Florida Wetlands Using ERS-1 SAR Imagery." *Photogrammetric Engineering & Remote Sensing* 63 (3): 281–291.

Kiage, L. M., N. D. Walker, S. Balasubramanian, A. Babin, and J. Barras. 2005. "Applications of Radarsat? 1 Synthetic Aperture Radar Imagery to Assess Hurricane?Related Flooding of Coastal

Louisiana." *International Journal of Remote Sensing* 26 (24): 5359–5380. doi:10.1080/01431160500442438.

Kittler, J., and J. Illingworth. 1986. "Minimum Error Thresholding." *Pattern Recognition* 19 (1): 41–47. doi:10.1016/0031-3203(86)90030-0.

Klemas, V. 2013. "Remote Sensing of Emergent and Submerged Wetlands: An Overview." *International Journal of Remote Sensing* 34 (18): 6286–6320. doi:10.1080/01431161.2013.800656.

Koch, M., T. Schmid, M. Reyes, and J. Gumuzzio. 2012. "Evaluating Full Polarimetric C- and L-Band Data for Mapping Wetland Conditions in a Semi-Arid Environment in Central Spain." *IEEE Journal Sel Topics Applications Earth Observations Remote Sensing* 5 (3): 1033–1044. doi:10.1109/JSTARS.2012.2202091.

Kuenzer, C., A. Bluemel, S. Gebhardt, T. V. Quoc, and S. Dech. 2011. "Remote Sensing of Mangrove Ecosystems. A Review." *Remote Sensing* 3 (12): 878–928. doi:10.3390/rs3050878.

Kwoun, O.-I., and L. Zhong. 2009. "Multi-Temporal RADARSAT-1 and ERS Backscattering Signatures of Coastal Wetlands in Southeastern Louisiana." *Photogramm Eng Remote Sensing* 75 (5): 607–617. doi:10.14358/PERS.75.5.607.

Lang, M. W., and E. S. Kasischke. 2008. "Using C-Band Synthetic Aperture Radar Data to Monitor Forested Wetland Hydrology in Maryland's Coastal Plain, USA." *IEEE Transactions Geoscience Remote Sensing* 46 (2): 535–546. doi:10.1109/TGRS.2007.909950.

Lang, M. W., E. S. Kasischke, S. D. Prince, and K. W. Pittman. 2008. "Assessment of C-Band Synthetic Aperture Radar Data for Mapping and Monitoring Coastal Plain Forested Wetlands in the Mid-Atlantic Region, U.S.A." *Remote Sensing of Environment* 112 (11): 4120–4130. doi:10.1016/j.rse.2007.08.026.

Lang, M. W., P. A. Townsend, and E. S. Kasischke. 2008. "Influence of Incidence Angle on Detecting Flooded Forests Using C-HH Synthetic Aperture Radar Data." *Remote Sensing of Environment* 112 (10): 3898–3907. doi:10.1016/j.rse.2008.06.013.

Le Toan, T., F. Ribbes, L.-F. Wang, N. Floury, K.-H. Ding, J. A. Kong, M. Fujita, and T. Kurosu. 1997. "Rice Crop Mapping and Monitoring Using ERS-1 Data Based on Experiment and Modeling Results." *IEEE Transactions Geoscience Remote Sensing* 35 (1): 41–56. doi:10.1109/36.551933.

Lee, H., T. Yuan, H. C. Jung, and E. Beighley. 2015. "Mapping Wetland Water Depths over the Central Congo Basin Using PALSAR ScanSAR, Envisat Altimetry, and MODIS VCF Data." *Remote Sensing of Environment* 159: 70–79. doi:10.1016/j.rse.2014.11.030.

Lee, J.-S., and E. Pottier. 2009. *Polarimetric Radar Imaging. From Basics to Applications*. Boca Raton: CRC Press (Optical science and engineering, 142).

Lewis, A. J., F. M. Henderson, and D. Holcomb. 1998. "Radar Fundamentals: The Geoscience Perspective." In *Principles and Applications of Imaging Radar*, 3rd ed. Vol. 2 edited by F. M. Henderson and A. J. Lewis, 131–181. New York: J. Wiley. (Manual of remote sensing).

Li, J., and W. Chen. 2005. "A Rule-Based Method for Mapping Canada's Wetlands Using Optical, Radar and DEM Data." *International Journal of Remote Sensing* 26 (22): 5051–5069. doi:10.1080/01431160500166516.

Li, S. Z. 2001. *Markov Random Field Modeling in Image Analysis*. Tokyo: Springer Japan (Computer Science Workbench).

Long, S., T. E. Fatoyinbo, and F. Policelli. 2014. "Flood Extent Mapping for Namibia Using Change Detection and Thresholding with SAR." *Environment Researcher Letters* 9 (3): 1–9. doi:10.1088/1748-9326/9/3/035002.

Lopes, A., R. Touzi, and E. Nezry. 1990. "Adaptive Speckle Filters and Scene Heterogeneity." *IEEE Transactions Geoscience Remote Sensing* 28 (6): 992–1000. doi:10.1109/36.62623.

Lu, Z., and O.-I. Kwoun. 2008. "Radarsat-1 and ERS InSAR Analysis over Southeastern Coastal Louisiana. Implications for Mapping Water-Level Changes beneath Swamp Forests." *IEEE Transactions Geoscience Remote Sensing* 46 (8): 2167–2184. doi:10.1109/TGRS.2008.917271.

Maillard, P., T. Alencar-Silva, and D. A. Clausi. 2008. "An Evaluation of Radarsat-1 and ASTER Data for Mapping Veredas (Palm Swamps)." *Sensors (Basel, Switzerland)* 8 (9): 6055–6076. doi:10.3390/s8096055.

Marti-Cardona, B., C. Lopez-Martinez, J. Dolz-Ripolles, and E. Bladè-Castellet. 2010. "ASAR Polarimetric, Multi-Incidence Angle and Multitemporal Characterization of Doñana Wetlands for Flood Extent Monitoring." *Remote Sensing of Environment* 114 (11): 2802–2815. doi:10.1016/j.rse.2010.06.015.

Marti-Cardona, B., J. Dolz-Ripolles, and C. Lopez-Martinez. 2013. "Wetland Inundation Monitoring by the Synergistic Use of ENVISAT/ASAR Imagery and Ancilliary Spatial Data." *Remote Sensing of Environment* 139: 171–184. doi:10.1016/j.rse.2013.07.028.

Martinez, J., and T. Le Toan. 2007. "Mapping of Flood Dynamics and Spatial Distribution of Vegetation in the Amazon Floodplain Using Multitemporal SAR Data." *Remote Sensing of Environment* 108 (3): 209–223. doi:10.1016/j.rse.2006.11.012.

Martinis, S., and A. Twele. 2010. "A Hierarchical Spatio-Temporal Markov Model for Improved Flood Mapping Using Multi-Temporal X-Band SAR Data." *Remote Sensing* 2 (9): 2240–2258. doi:10.3390/rs2092240.

Martinis, S., and C. Rieke. 2015. "Backscatter Analysis Using Multi-Temporal and Multi-Frequency SAR Data in the Context of Flood Mapping at River Saale, Germany." *Remote Sensing* 7 (6): 7732–7752. doi:10.3390/rs70607732.

Mayaux, P., G. F. de Grandi, Y. Rauste, M. Simard, and S. Saatchi. 2002. "Large-Scale Vegetation Maps Derived from the Combined L-Band GRFM and C-Band CAMP Wide Area Radar Mosaics of Central Africa." *International Journal of Remote Sensing* 23 (7): 1261–1282. doi:10.1080/01431160110092894.

Melack, J. M., and L. L. Hess. 2010. "Remote Sensing of the Distributions and Extent of Wetlands in the Amazon Basin." In *Amazonian Flodplain Forests: Ecophysiology, Ecology, Biodiversity and Sustainable Management: Ecological Studies*, edited by W. J. Junk, M. Piedade, F. Wittmann, P. Parolin, and J. Schöngart, 43–59, Netherlands: Springer.

Melack, J. M., and Y. Wang. 1998. "Delineation of Flooded Area and Flooded Vegetation in Balbina Reservoir (Amazonas, Brazil) with Synthetic Aperture Radar." *Erhandlungen - Internationale Vereinigung Fur Theoretische Und Angewandte Limnologie* 26: 2374–2377.

Millennium Ecosystem Assessment. 2005. *Ecosystems and Human Well-Being: Synthesis*. Washington, DC: Island Press.

Miranda, F. P., L. E. N. Fonseca, and J. R. Carr. 1998. "Semivariogram Textural Classification of JERS-1 (Fuyo-1) SAR Data Obtained over a Flooded Area of the Amazon Rainforest." *International Journal of Remote Sensing* 19 (3): 549–556. doi:10.1080/014311698216170.

Mishra, D. R., S. Ghosh, C. Hladik, J. L. O'Connell, and H. J. Cho. 2016. "Wetland Mapping Methods and Techniques Using Multisensor, Multiresolution Remote Sensing: Successes and Challenges." In *Remote Sensing of Water Resources, Disasters, and Urban Studies*, edited by P. S. Thenkabail, 191–220. Boca Raton: CRC Press (Remote sensing handbook).

Morandeira, N., F. Grings, C. Facchinetti, and P. Kandus. 2016. "Mapping Plant Functional Types in Floodplain Wetlands. An Analysis of C-Band Polarimetric SAR Data from RADARSAT-2." *Remote Sensing* 8 (3): 174. doi:10.3390/rs8030174.

Moser, L., A. Schmitt, A. Wendleder, and A. Roth. 2016. "Monitoring of the Lac Bam Wetland Extent Using Dual-Polarized X-Band SAR Data." *Remote Sensing* 8 (4): 302. doi:10.3390/rs8040302.

Mougin, E., C. Proisy, G. Marty, F. Fromard, H. Puig, J. L. Betoulle, and J. P. Rudant. 1999. "Multifrequency and Multipolarization Radar Backscattering from Mangrove Forests." *IEEE Transactions Geoscience Remote Sensing* 37 (1): 94–102. doi:10.1109/36.739128.

Mwita, E., G. Menz, S. Misana, and P. Nienkemper. 2012. "Detection of Small Wetlands with Multi Sensor Data in East Africa." *ARS* 01 (03): 64–73. doi:10.4236/ars.2012.13007.

Na, X., S. Zang, L. Liu, and M. Li. 2013. "Wetland Mapping in the Zhalong National Natural Reserve, China, Using Optical and Radar Imagery and Topographical Data." *Journal Applications Remote Sens* 7 (1): 73554. doi:10.1117/1.JRS.7.073554.

Na, X. D., S. Y. Zang, C. S. Wu, and W. L. Li. 2015. "Mapping Forested Wetlands in the Great Zhan River Basin through Integrating Optical, Radar, and Topographical Data Classification Techniques." *Environmental Monitoring and Assessment* 187 (11): 696. doi:10.1007/s10661-015-4914-7.

Nord, M. E., T. L. Ainsworth, J.-S. Lee, and N. J. S. Stacy. 2009. "Comparison of Compact Polarimetric Synthetic Aperture Radar Modes." *IEEE Transactions Geoscience Remote Sensing* 47 (1): 174–188. doi:10.1109/TGRS.2008.2000925.

Oliver-Cabrera, T., and S. Wdowinski. 2016. "InSAR-Based Mapping of Tidal Inundation Extent and Amplitude in Louisiana Coastal Wetlands." *Remote Sensing* 8 (5): 393. doi:10.3390/rs8050393.

Otsu, N. 1979. "A Threshold Selection Method from Gray-Level Histograms." *IEEE Transactions on Systems, Man, and Cybernetics* 9: 62–66. doi:10.1109/TSMC.1979.4310076.

Park, H.-S., and C.-H. Jun. 2009. "A Simple and Fast Algorithm for K-Medoids Clustering." *Expert Systems with Applications* 36 (2): 3336–3341. doi:10.1016/j.eswa.2008.01.039.

Patel, P., H. Srivastava, and R. Navalgund. 2009. "Use of Synthetic Aperture Radar Polarimetry to Characterize Wetland Targets of Keoladeo National Park, Bharatpur, India." *Current Science* 97 (4): 529–537.

Pierdicca, N., L. Pulvirenti, M. Chini, L. Guerriero, and L. Candela. 2013. "Observing Floods from Space: Experience Gained from COSMO-SkyMed Observations." *Acta Astronautica* 84: 122–133. doi:10.1016/j.actaastro.2012.10.034.

Pierdicca, N., M. Chini, L. Pulvirenti, and F. Macina. 2008. "Integrating Physical and Topographic Information into a Fuzzy Scheme to Map Flooded Area by SAR." *Sensors* 8 (7): 4151–4164. doi:10.3390/s8074151.

Pistolesi, L. I., W. Ni-Meister, and K. C. McDonald. 2015. "Mapping Wetlands in the Hudson Highlands Ecoregion with ALOS PALSAR. An Effort to Identify Potential Swamp Forest Habitat for Golden-Winged Warblers." *Wetlands Ecology Manage* 23 (1): 95–112. doi:10.1007/s11273-014-9381-3.

Podest, E., and S. Saatchi. 2002. "Application of Multiscale Texture in Classifying JERS-1 Radar Data over Tropical Vegetation." *International Journal of Remote Sensing* 23 (7): 1487–1506. doi:10.1080/01431160110093000.

Pope, K. O., E. Rejmankova, and J. F. Paris. 2001. "Spaceborne Imaging radar-C (SIR-C) Observations of Groundwater Discharge and Wetlands Associated with the Chicxulub Impact Crater, Northwestern Yucatan Peninsula, Mexico." *Geological Society of America Bulletin* 113 (3): 403–416. doi:10.1130/0016-7606(2001)113<0403:SIRCSC>2.0.CO;2.

Pope, K. O., E. Rejmankova, J. F. Paris, and R. Woodruff. 1997. "Detecting Seasonal Flooding Cycles in Marshes of the Yucatan Peninsula with SIR-C Polarimetric Radar Imagery." *Remote Sensing of Environment* 59 (2): 157–166. doi:10.1016/S0034-4257(96)00151-4.

Pope, K. O., J. M. Rey-Benayas, and J. F. Paris. 1994. "Radar Remote Sensing of Forest and Wetland Ecosystems in the Central American Tropics." *Remote Sensing of Environment* 48 (2): 205–219. doi: 10.1016/0034-4257(94)90142-2.

Pulvirenti, L., M. Chini, N. Pierdicca, and G. Boni. 2016. "Use of SAR Data for Detecting Floodwater in Urban and Agricultural Areas: The Role of the Interferometric Coherence." *IEEE Transactions Geoscience Remote Sensing* 54 (3): 1532–1544. doi:10.1109/TGRS.2015.2482001.

Pulvirenti, L., M. Chini, N. Pierdicca, L. Guerriero, and P. Ferrazzoli. 2011a. "Flood Monitoring Using Multi-Temporal COSMO-SkyMed Data. Image Segmentation and Signature Interpretation." *Remote Sensing of Environment* 115 (4): 990–1002. doi:10.1016/j.rse.2010.12.002.

Pulvirenti, L., N. Pierdicca, and M. Chini. 2010. "Analysis of Cosmo-SkyMed Observations of the 2008 Flood in Myanmar." *ItJRS* 79–90. doi:10.5721/ItJRS20104217.

Pulvirenti, L., N. Pierdicca, M. Chini, and L. Guerriero. 2011b. "An Algorithm for Operational Flood Mapping from Synthetic Aperture Radar (SAR) Data Using Fuzzy Logic." *Natural Hazards Earth Systems Sciences* 11 (2): 529–540. doi:10.5194/nhess-11-529-2011.

Pulvirenti, L., N. Pierdicca, M. Chini, and L. Guerriero. 2013. "Monitoring Flood Evolution in Vegetated Areas Using COSMO-SkyMed Data: The Tuscany 2009 Case Study." *IEEE Journal Sel Topics Applications Earth Observations Remote Sensing* 6 (4): 1807–1816. doi:10.1109/JSTARS.2012.2219509.

Quegan, S., and J. Yu. 2001. "Filtering of Multichannel SAR Images." *IEEE Transactions Geoscience Remote Sensing* 39 (11): 2373–2379. doi:10.1109/36.964973.

Rebelo, L.-M., G. B. Senay, and M. P. McCartney. 2012. "Flood Pulsing in the Sudd Wetland: Analysis of Seasonal Variations in Inundation and Evaporation in South Sudan." *Earth Interact* 16 (1): 1–19. doi:10.1175/2011EI382.1.

Richards, J. A. 2012. *Remote Sensing Digital Image Analysis. An Introduction*. 5th ed. Berlin, New York: Springer.

Richards, J. A., P. W. Woodgate, and A. K. Skidmore. 1987. "An Explanation of Enhanced Radar Backscattering from Flooded Forests." *International Journal of Remote Sensing* 8 (7): 1093–1100. doi:10.1080/01431168708954756.

Rignot, E. J. M., and J. J. van Zyl. 1993. "Change Detection Techniques for ERS-1 SAR Data." *IEEE Transactions Geoscience Remote Sensing* 31 (4): 896–906. doi:10.1109/36.239913.

Robertson, L. D., D. J. King, and C. Davies. 2015. "Object-Based Image Analysis of Optical and Radar Variables for Wetland Evaluation." *International Journal of Remote Sensing* 36 (23): 5811–5841. doi:10.1080/01431161.2015.1109727.

Rodrigues, S. W. P., and P. W. M. Souza-Filho. 2011. "Use of Multi-Sensor Data to Identify and Map Tropical Coastal Wetlands in the Amazon of Northern Brazil." *Wetlands* 31 (1): 11–23. doi:10.1007/s13157-010-0135-6.

Rosenqvist, A., C. M. Finlayson, J. Lowry, and D. Taylor. 2007. "The Potential of Long-Wavelength Satellite-Borne Radar to Support Implementation of the Ramsar Wetlands Convention." *Aquatic Conservatin: Marine. Freshwater Ecosystem* 17 (3): 229–244. doi:10.1002/aqc.835.

Sang, H., J. Zhang, H. Lin, and L. Zhai. 2014. "Multi-Polarization ASAR Backscattering from Herbaceous Wetlands in Poyang Lake Region, China." *Remote Sensing* 6 (5): 4621–4646. doi:10.3390/rs6054621.

Schlaffer, S., M. Chini, D. Dettmering, and W. Wagner. 2016. "Mapping Wetlands in Zambia Using Seasonal Backscatter Signatures Derived from ENVISAT ASAR Time Series." *Remote Sensing* 8: 5. doi:10.3390/rs8050402.

Schmitt, A., A. Wendleder, and S. Hinz. 2015. "The Kennaugh Element Framework for Multi-Scale, Multi-Polarized, Multi-Temporal and Multi-Frequency SAR Image Preparation." *ISPRS Journal of Photogrammetry and Remote Sensing* 102: 122–139. doi:10.1016/j.isprsjprs.2015.01.007.

Schmitt, A., and B. Brisco. 2013. "Wetland Monitoring Using the Curvelet-Based Change Detection Method on Polarimetric SAR Imagery." *Water* 5 (3): 1036–1051. doi:10.3390/w5031036.

Schmitt, A., B. Wessel, and A. Roth. 2010. "Curvelet-Based Change Detection on SAR Images for Natural Disaster Mapping." *Photogrammetrie-Fernerkundung-Geoinformation* 2010 (6): 463–474. doi:10.1127/1432-8364/2010/0068.

Schmitt, A., T. Leichtle, M. Huber, and A. Roth. 2012. "On the Use of Dual-Co-Polarized TerraSAR-X Data for Wetland Monitoring." *International Archives Photogramm Remote Sens Spatial Information Sciences* XXXIX-B7: 341–344. doi:10.5194/isprsarchives-XXXIX-B7-341-2012.

Schmullius, C. C., and D. L. Evans. 1997. "Review Article Synthetic Aperture Radar (SAR) Frequency and Polarization Requirements for Applications in Ecology, Geology, Hydrology, and Oceanography: A Tabular Status Quo after SIR-C/X-SAR." *International Journal of Remote Sensing* 18 (13): 2713–2722. doi:10.1080/014311697217297.

Schumann, G., G. Di Baldassarre, and P. D. Bates. 2009. "The Utility of Spaceborne Radar to Render Flood Inundation Maps Based on Multialgorithm Ensembles." *IEEE Transactions Geoscience Remote Sensing* 47 (8): 2801–2807. doi:10.1109/TGRS.2009.2017937.

Schumann, G. J.-P., and D. K. Moller. 2015. "Microwave Remote Sensing of Flood Inundation." *Physics and Chemistry of the Earth, Parts A/B/C* 83-84: 84–95. doi:10.1016/j.pce.2015.05.002.

Silva, T. S., F. Costa, P. F. Maycira, J. M. Melack, and E. M. L. M. Novo. 2008. "Remote Sensing of Aquatic Vegetation: Theory and Applications." *Environmental Monitoring and Assessment* 140 (1–3): 131–145. doi:10.1007/s10661-007-9855-3.

Simard, M., G. de Grandi, S. Saatchi, and P. Mayaux. 2002. "Mapping Tropical Coastal Vegetation Using JERS-1 and ERS-1 Radar Data with a Decision Tree Classifier." *International Journal of Remote Sensing* 23 (7): 1461–1474. doi:10.1080/01431160110092984.

Simard, M., S. S. Saatchi, and G. de Grandi. 2000. "The Use of Decision Tree and Multiscale Texture for Classification of JERS-1 SAR Data over Tropical Forest." *IEEE Transactions Geoscience Remote Sensing* 38 (5): 2310–2321. doi:10.1109/36.868888.

Souza-Filho, P. W. M., W. R. Paradella, S. W. P. Rodrigues, F. R. Costa, J. C. Mura, and F. D. Gonçalves. 2011. "Discrimination of Coastal Wetland Environments in the Amazon Region Based on Multi-Polarized L-Band Airborne Synthetic Aperture Radar Imagery." *Estuarine, Coastal and Shelf Science* 95 (1): 88–98. doi:10.1016/j.ecss.2011.08.011.

Touzi, R., A. Deschamps, and G. Rother. 2007. "Wetland Characterization Using Polarimetric RADARSAT-2 Capability." *Canadian Journal of Remote Sensing* 33: S56–S67. doi:10.5589/m07-047.

Touzi, R., A. Deschamps, and G. Rother. 2009. "Phase of Target Scattering for Wetland Characterization Using Polarimetric C-Band SAR." *IEEE Transactions Geoscience Remote Sensing* 47 (9): 3241–3261. doi:10.1109/TGRS.2009.2018626.

Townsend, P. A. 2001. "Mapping Seasonal Flooding in Forested Wetlands Using Multi-Temporal Radarsat SAR." *Photogrammetric Engineering & Remmote Sensing* 67 (7): 857–864.

Townsend, P. A. 2002. "Relationships between Forest Structure and the Detection of Flood Inundation in Forested Wetlands Using C-Band SAR." *International Journal of Remote Sensing* 23 (3): 443–460. doi:10.1080/01431160010014738.

Töyrä, J., A. Pietroniro, and L. W. Martz. 2001. "Multisensor Hydrologic Assessment of a Freshwater Wetland." *Remote Sensing of Environment* 75 (2): 162–173. doi:10.1016/S0034-4257(00)00164-4.

Töyrä, J., A. Pietroniro, L. W. Martz, and T. D. Prowse. 2002. "A Multi-Sensor Approach to Wetland Flood Monitoring." *Hydrology Processing* 16 (8): 1569–1581. doi:10.1002/hyp.1021.

Trujillo, M. 2015. "The impact of disasters on agriculture and food security." Rome, Italy: Food and Agriculture Organization of the United Nations

Ulaby, F. T., A. K. Fung, and R. K. Moore. 1986. *Microwave Remote Sensing: Active and Passiv. Volume II: Radar Remote Sensing and Surface Scattering and Emission Theory*. Norwood, MA: Artech House (Remote sensing).

Ulaby, F. T., and M. C. Dobson. 1989. *Handbook of Radar Scattering Statistics for Terrain*. Norwood, MA: Artech House (The Artech House remote sensing library).

Voormansik, K., J. Praks, O. Antropov, J. Jagomagi, and K. Zalite. 2014. "Flood Mapping with TerraSAR-X in Forested Regions in Estonia." *IEEE Journal Sel Topics Applications Earth Observations Remote Sensing* 7 (2): 562–577. doi:10.1109/JSTARS.2013.2283340.

Wang, J., J. Shang, B. Brisco, and R. J. Brown. 1998. "Evaluation of Multidate ERS-1 and Multispectral Landsat Imagery for Wetland Detection in Southern Ontario." *Canadian Journal of Remote Sensing* 24 (1): 60–68. doi:10.1080/07038992.1998.10874692.

Wang, Y. 2002. "Mapping Extent of Floods. What We Have Learned and How We Can Do Better." *Natural Hazards Reviews* 3 (2): 68–73. doi:10.1061/(ASCE)1527-6988(2002)3:2(68).

Wang, Y. 2004. "Seasonal Change in the Extent of Inundation on Floodplains Detected by JERS-1 Synthetic Aperture Radar Data." *International Journal of Remote Sensing* 25 (13): 2497–2508. doi:10.1080/01431160310001619562.

Wang, Y., and F. W. Davis. 1997. "Decomposition of Polarimetric Synthetic Aperture Radar Backscatter from Upland and Flooded Forests." *International Journal of Remote Sensing* 18 (6): 1319–1332. doi:10.1080/014311697218449.

Wang, Y., L. L. Hess, S. Filoso, and J. M. Melack. 1995. "Understanding the Radar Backscattering from Flooded and Nonflooded Amazonian Forests. Results from Canopy Backscatter Modeling." *Remote Sensing of Environment* 54 (3): 324–332. doi:10.1016/0034-4257(95)00140-9.

Ward, D. P., A. Petty, S. A. Setterfield, M. M. Douglas, K. Ferdinands, S. K. Hamilton, and S. Phinn. 2014. "Floodplain Inundation and Vegetation Dynamics in the Alligator Rivers Region (Kakadu) of Northern Australia Assessed Using Optical and Radar Remote Sensing." *Remote Sensing of Environment* 147: 43–55. doi:10.1016/j.rse.2014.02.009.

Wdowinski, S., W. Kim, F. Amelung, and T. Dixon. 2006. *Wetland InSAR: A New Space-Based Hydrological Monitoring Tool of Wetlands Surface Water Level Changes*, SP–634. Frescati, Italy: European Space Agency, (Special Publication) ESA SP.

Westra, T. 2010. "Optimal Envisat Advanced Synthetic Aperture Radar Image Parameters for Mapping and Monitoring Sahelian Floodplains." *Journal Applications Remote Sens* 4 (1): 43511. doi:10.1117/1.3368722.

Whitcomb, J., M. Moghaddam, K. McDonald, J. Kellndorfer, and E. Podest. 2009. "Mapping Vegetated Wetlands of Alaska Using L-Band Radar Satellite Imagery." *Canadian Journal of Remote Sensing* 35 (1): 54–72. doi:10.5589/m08-080.

White, L., B. Brisco, M. Dabboor, A. Schmitt, and A. Pratt. 2015. "A Collection of SAR Methodologies for Monitoring Wetlands." *Remote Sensing* 7 (6): 7615–7645. doi:10.3390/rs70607615.

White, L., B. Brisco, M. Pregitzer, B. Tedford, and L. Boychuk. 2014. "RADARSAT-2 Beam Mode Selection for Surface Water and Flooded Vegetation Mapping." *Canadian Journal of Remote Sensing* 40: 135–151.

Xie, C., Y. Shao, X. Ji, Z. Wan, and L. Fang. 2013. "Analysis of ALOS PALSAR InSAR Data for Mapping Water Level Changes in Yellow River Delta Wetlands." *International Journal of Remote Sensing* 34 (6): 2047–2056. doi:10.1080/01431161.2012.731541.

Yu, Y., and S. Saatchi. 2016. "Sensitivity of L-Band SAR Backscatter to Aboveground Biomass of Global Forests." *Remote Sensing* 8 (6): 522. doi:10.3390/rs8060522.

Zhang, M., L. Zhen, B. Tian, J. Zhou, and P. Tang. 2016. "The Backscattering Characteristics of Wetland Vegetation and Water-Level Changes Detection Using Multi-Mode SAR. A Case Study." *International Journal of Applied Earth Observation and Geoinformation* 45: 1–13. doi:10.1016/j.jag.2015.10.001.

Zhang, M., Z. Li, B. Tian, J. Zhou, and J. Zeng. 2015. "A Method for Monitoring Hydrological Conditions beneath Herbaceous Wetlands Using Multi-Temporal ALOS PALSAR Coherence Data." *International Archives Photogramm Remote Sensing Spatial Information Sciences* XL-7/W4: 221–226. doi:10.5194/isprsarchives-XL-7-W4-221-2015.

Zhao, L., J. Yang, L. Pingxiang, and L. Zhang. 2014. "Seasonal Inundation Monitoring and Vegetation Pattern Mapping of the Erguna Floodplain by Means of a RADARSAT-2 Fully Polarimetric Time Series." *Remote Sensing of Environment* 152: 426–440. doi:10.1016/j.rse.2014.06.026.

Appendix 1.

1	Allen, Wang, and Gore (2013)	31	Cremon, Rossetti, Dilce, and Zani (2014)	61	Lee et al. (2015)
2	Alsdorf et al. (2000)	32	Dabboor et al. (2015)	62	Le Toan et al. (1997)
3	Alsdorf, Smith, and Melack (2001)	33	De Grandi et al. (2000)	63	Li and Chen (2005)
4	Arnesen et al. (2013)	34	Dwivedi, Rao, and Bhattacharya (1999)	64	Long, Fatoyinbo, and Policelli (2014)
5	Augusteijn and Warrender (1998)	35	Evans et al. (2010)	65	Lu and Kwoun (2008)
6	Aziz and White (2003)	36	Evans and Costa (2013)	66	Maillard, Alencar-Silva, and Clausi (2008)
7	Baghdadi et al. (2001)	37	Evans et al. (2014)	67	Marti-Cardona et al. (2010)
8	Betbeder et al. (2014)	38	Ferreira-Ferreira et al. (2015)	68	Marti-CardoMarti-Cardona, Dolz-Ripolles, and Lopez-Martinez (2013)
9	Betbeder et al. (2015)	39	Frappart et al. (2005)	69	Martinez and Le Toan (2007)
10	Bian et al. (2016)	40	Furtado, Silva, and Novo (2016)	70	Martinis and Twele (2010)
11	Bourgeau-Chavez, Kasischke, and Smith (1997)	41	Gallant et al. (2014)	71	Martinis and Rieke (2015)
12	Bourgeau-Chavez et al. (2001)	42	Grenier et al. (2007)	72	Mayaux et al. (2002)
13	Bourgeau-Chavez et al. (2009)	43	Grings et al. (2006)	73	Melack and Wang (1998)
14	Bourgeau-Chavez et al. (2016)	44	Grings et al. (2008)	74	Miranda, Fonseca, and Carr (1998)
15	(Bouvet and Le Toan 2011)	45	Heine, Jagdhuber, and Itzerott (2016)	75	Morandeira et al. (2016)
16	Brisco et al. (2008)	46	Hess et al. (1995)	76	Moser et al. (2016)
17	Brisco et al. (2011)	47	Hess and Melack (2003)	77	Mougin et al. (1999)
18	Brisco et al. (2013a)	48	Hess et al. (2003)	78	Mwita et al. (2012)
19	Brisco et al. (2013b)	49	Hess et al. (2015)	79	Na et al. (2013)
20	Brown, Mwansasu, and Westerberg (2016)	50	Hidayat et al. (2012)	80	Na et al. (2015)
21	Bwangoy et al. (2010)	51	Horritt (2003)	81	Oliver-Cabrera and Wdowinski (2016)
22	Cazals et al. (2016)	52	Imhoff et al. (1986)	82	Patel, Srivastava, and Navalgund (2009)
23	Chapman et al. (2015)	53	Kandus et al. (2001)	83	Pierdicca et al. (2008)
24	Chen et al. (2014)	54	Karszenbaum et al. (2000)	84	Pierdicca et al. (2013)
25	Corcoran et al. (2012)	55	Kasischke and Bourgeau-Chavez (1997)	85	Pistolesi, Ni-Meister, and McDonald (2015)
26	Cordeiro and Rossetti (2015)	56	Kasischke et al. (2003)	86	Podest and Saatchi (2002)
27	Costa et al. (1997)	57	Kiage et al. (2005)	87	Pope, Rey-Benayas, and Paris (1994)
28	Costa et al. (2002)	58	Kwoun and Lu (2009)	88	Pope et al. (1997)
29	Costa (2004)	59	Lang and Kasischke (2008)	89	Pope, Rejmankova, and Paris (2001)
30	Costa and Telmer (2006)	60	Lang et al. (2008)	90	Pulvirenti, Pierdicca, and Chini (2010)

(*Continued*)

(Continued).

91	Pulvirenti et al. (2011a)	110	Townsend (2002)
92	Pulvirenti et al. (2011b)	111	Töyra et al. (2001)
93	Pulvirenti et al. (2013)	112	Töyra et al. (2002)
94	Pulvirenti et al. (2016)	113	Voormansik et al. (2014)
95	Rebelo, Senay, and McCartney (2012)	114	Wang et al. (1995)
96	Richards et al. (1987)	115	Wang and Davis (1997)
97	Robertson, King, and Davies (2015)	116	Wang et al. (1998)
98	Rodrigues and Souza-Filho (2011)	117	Wang (2002)
99	Rosenqvist et al. (2007)	118	Wang (2004)
100	Sang et al. (2014)	119	Ward et al. (2014)
101	Schlaffer et al. (2016)	120	Wdowinski et al. (2006)
102	Schmitt, Wessel, and Roth (2010)	121	Westra (2010)
103	Schmitt and Brisco (2013)	122	Whitcomb et al. (2009)
104	Simard, Saatchi, and De Grandi (2000)	123	White et al. (2014)
105	Simard et al. (2002)	124	Xie et al. (2013)
106	Souza-Filho et al. (2011)	125	Yu and Saatchi (2016)
107	Touzi, Deschamps, and Rother (2007)	126	Zhang et al. (2015)
108	Touzi, Deschamps, and Rother (2009)	127	Zhang et al. (2016)
109	Townsend (2001)	128	Zhao et al. (2014)

List of studies (128 articles) analysed in this review.
The IDs in Appendix 1 do not correspond to the study IDs in Table 2.